THE ASTRONOMICAL JOURNAL

PUBLISHED BY THE AMERICAN INSTITUTE OF PHYSICS
FOR THE AMERICAN ASTRONOMICAL SOCIETY

VOLUME 65 1960 October ~ No. 1283 *NUMBER 8*

Osculating Elements Derived from the Modified Hansen Theory for the Motion of an Artificial Satellite

A. Bailie and R. Bryant

Theoretical Division, Goddard Space Flight Center, National Aeronautics and Space Administration, Washington, D. C.

(Received June 15, 1960)

The modified Hansen theory for the motion of an artificial satellite, as developed by Peter Musen, represents the gravitational perturbations. The development takes the form of several trigonometric series with numerical coefficients and specified arguments. The result of the modified Hansen theory is the position vector of the satellite which is obtained by evaluating these series.

In the present paper the velocity vector and the six classical osculating elements are shown to be obtainable also from the series in the general theory.

The ability to obtain osculating elements and/or velocity from the modified Hansen theory is considered a significant adjunct to that theory. Comparison with other general perturbations theories and with special perturbations techniques is now possible. Accurate transition from the general theory to numerical integration makes it possible to transfer to the latter method when additional disturbing forces, not included in the general theory, become of consequence.

INTRODUCTION

THE modified Hansen theory (Musen 1959) represents the gravitational perturbations of an rtificial satellite. The development takes the form of everal trigonometric series with numerical coefficients nd specified arguments. The result of the modified Hansen theory is the position vector of the satellite hich is obtained by evaluating these series. The resent paper contains the derivation of the velocity ector and the osculating elements from this theory. comparison of the results of the modified Hansen heory with those of other general perturbations heories and with those of numerical integration is ow possible.

DETERMINATION OF THE VECTORIAL CONSTANTS FOR THE EQUATOR

A basic trihedron, (**P**,**Q**,**R**), connected with the sculating plane is represented by the vector toward erigee, **P**, one directed perpendicular to the orbit, **R**, nd a third, **Q**, at right angles to **P** and **R**, and forming ith them a right-handed system. The components of hese unit vectors are, in terms of the Keplerian elements:

$$\mathbf{P}=\begin{bmatrix}-\cos i\,\sin\omega\,\sin\theta+\cos\omega\,\cos\theta\\+\cos i\,\sin\omega\,\cos\theta+\cos\omega\,\sin\theta\\+\sin i\,\cos\omega\end{bmatrix} \tag{1}$$

$$\mathbf{Q}=\begin{bmatrix}-\cos i\,\cos\omega\,\sin\theta-\sin\omega\,\cos\theta\\+\cos i\,\cos\omega\,\cos\theta-\sin\omega\,\sin\theta\\+\sin i\,\cos\omega\end{bmatrix} \tag{2}$$

$$\mathbf{R}=\begin{bmatrix}+\sin i\,\sin\theta\\-\sin i\,\cos\theta\\+\cos i\end{bmatrix}. \tag{3}$$

Taking the following relations into consideration, (Musen 1959) which represent a modification of Hansen's basic relations (Hansen 1862):

$$\omega=\chi-\sigma$$
$$\sigma=\sigma_0-(\alpha-\eta)\Delta E-N-K$$
$$\theta=\theta_0-(\alpha+\eta)\Delta E-N+K,$$

and using the "mean" or Hansen values of ω and θ,

$$(\omega)=\pi_0-\sigma_0+(\gamma+\alpha-\eta)\Delta E \tag{4}$$

$$(\theta)=\theta_0-(\alpha+\eta)\Delta E, \tag{5}$$

the developments for the osculating values of **P**, **Q**,

and **R** are easily obtained. As an example of the result we give the development for P_x:

$$\begin{aligned}P_x=&+\cos^2\tfrac{1}{2}i\cos 2K\cos[\chi-\pi_0-y\Delta E+(\omega)+(\theta)]\\&-\cos^2\tfrac{1}{2}i\sin 2K\sin[\chi-\pi_0-y\Delta E+(\omega)+(\theta)]\\&+\sin^2\tfrac{1}{2}i\cos 2N\cos[\chi-\pi_0-y\Delta E+(\omega)-(\theta)]\\&-\sin^2\tfrac{1}{2}i\sin 2N\sin[\chi-\pi_0-y\Delta E+(\omega)-(\theta)].\end{aligned}$$

From Eq. (16) of the "Application of Hansen's Theory," (Musen 1959) the osculating values of the λ parameters are

$$\lambda_1=\sin\tfrac{1}{2}i\cos N \quad \lambda_3=\cos\tfrac{1}{2}i\sin K$$
$$\lambda_2=\sin\tfrac{1}{2}i\sin N \quad \lambda_4=\cos\tfrac{1}{2}i\cos K,$$

and their numerical values are obtained by evaluating their respective series. Defining

$$\beta=e\cos(\chi-\pi_0-y\Delta E) \tag{6}$$

$$\gamma=e\sin(\chi-\pi_0-y\Delta E), \tag{7}$$

we see that

$$\begin{aligned}eP_x=&\beta\{(\lambda_4^2-\lambda_3^2)\cos[(\omega)+(\theta)]-2\lambda_3\lambda_4\sin[(\omega)+(\theta)]\\&+(\lambda_1^2-\lambda_2^2)\cos[(\omega)-(\theta)]-2\lambda_1\lambda_2\sin[(\omega)-(\theta)]\}\\&-\gamma\{(\lambda_4^2-\lambda_3^2)\sin[(\omega)+(\theta)]+2\lambda_3\lambda_4\cos[(\omega)+(\theta)]\\&+(\lambda_1^2-\lambda_2^2)\sin[(\omega)-(\theta)]+2\lambda_1\lambda_2\cos[(\omega)-(\theta)]\}.\end{aligned}$$

We also obtain similar expressions for the y and z components of osculating $e\mathbf{P}$ and for the components of $e\mathbf{Q}$. We then define (**P**) and (**Q**) to be the coefficients of β in the expressions for $e\mathbf{P}$ and $e\mathbf{Q}$, respectively. This is done for two reasons. (1) We know χ to be the angle from X, the departure point, to the osculating perigee and $\pi_0+y\Delta E$ to be the same angle for the auxiliary ellipse to the perigee of the auxiliary ellipse. Hence $\chi-\pi_0-y\Delta E$ is small and of the order of the perturbations, β is of the order of e, γ is approximately zero and (**P**) approaches the real value of **P**. (2) We note the following relationships exist:

$$e\mathbf{P}=\beta(\mathbf{P})+\gamma(\mathbf{Q}) \tag{8}$$

$$e\mathbf{Q}=\beta(\mathbf{Q})-\gamma(\mathbf{P}). \tag{9}$$

We define $(\mathbf{R})=\mathbf{R}$ since **R** does not contain β or γ.

One of the results of the Hansen theory is a trigonometric series,

$$W=X+Y\sin F+Z\cos F,$$

where X comprises those terms in W independent of F, and Y and Z are composed of the terms in W which have a coefficient for F of ± 1 in the argument. We can obtain Y and Z easily by evaluating the series $W-X$ at $F=0$ for Y, and at $F=\frac{1}{2}\pi$ for Z. Using the expressions for Y and Z (Hansen 1838)

$$Y=2\left(\frac{h}{h_0}\right)\frac{e\cos(\chi-\pi_0-y\Delta E)-e_0}{1-e_0^2} \tag{10}$$

$$Z=2\left(\frac{h}{h_0}\right)\frac{e\sin(\chi-\pi_0-y\Delta E)}{(1-e_0^2)^{\frac{1}{2}}}, \tag{11}$$

we can easily obtain β and γ.

$$\beta=e_0+\frac{h_0}{h}\frac{(1-e_0^2)}{2}Y \tag{1}$$

$$\gamma=\frac{h_0}{h}\frac{(1-e_0^2)^{\frac{1}{2}}}{2}Z. \tag{1}$$

Finally, in order to obtain the osculating values of **Q** and **R**, we have

$$\begin{aligned}(P_x)=&+(\lambda_4^2-\lambda_3^2)\cos[(\omega)+(\theta)]\\&-2\lambda_3\lambda_4\sin[(\omega)+(\theta)]\\&+(\lambda_1^2-\lambda_2^2)\cos[(\omega)-(\theta)]\\&-2\lambda_1\lambda_2\sin[(\omega)-(\theta)]\\(P_y)=&+(\lambda_4^2-\lambda_3^2)\sin[(\omega)+(\theta)]\\&+2\lambda_3\lambda_4\cos[(\omega)+(\theta)]\\&-(\lambda_1^2-\lambda_2^2)\sin[(\omega)-(\theta)]\\&-2\lambda_1\lambda_2\cos[(\omega)-(\theta)]\\(P_z)=&+2(\lambda_1\lambda_4-\lambda_2\lambda_3)\sin(\omega)\\&+2(\lambda_2\lambda_4+\lambda_1\lambda_3)\cos(\omega)\\(Q_x)=&-(\lambda_4^2-\lambda_3^2)\sin[(\omega)+(\theta)]\\&-2\lambda_3\lambda_4\cos[(\omega)+(\theta)]\\&-(\lambda_1^2-\lambda_2^2)\sin[(\omega)-(\theta)]\\&-2\lambda_1\lambda_2\cos[(\omega)-(\theta)]\\(Q_y)=&+(\lambda_4^2-\lambda_3^2)\cos[(\omega)+(\theta)]\\&-2\lambda_3\lambda_4\sin[(\omega)+(\theta)]\\&-(\lambda_1^2-\lambda_2^2)\cos[(\omega)-(\theta)]\\&+2\lambda_1\lambda_2\sin[(\omega)-(\theta)]\\(Q_z)=&+2(\lambda_1\lambda_4-\lambda_2\lambda_3)\cos(\omega)-2(\lambda_2\lambda_4+\lambda_1\lambda_3)\sin(\omega)\\(R_x)=&+2(\lambda_1\lambda_4+\lambda_2\lambda_3)\sin(\theta)-2(\lambda_2\lambda_4-\lambda_1\lambda_3)\cos(\theta)\\(R_y)=&-2(\lambda_1\lambda_4+\lambda_2\lambda_3)\cos(\theta)-2(\lambda_2\lambda_4-\lambda_1\lambda_3)\sin(\theta)\\(R_z)=&(\lambda_4^2+\lambda_3^2-\lambda_2^2-\lambda_1^2).\end{aligned}$$

It is interesting to note that the above nine values (**P**), (**Q**) and (**R**) are nothing more than the n components of the Γ-matrix (Musen 1959) which used to rotate the auxiliary $\bar{\mathbf{r}}$ from the auxiliary (**Q**), (**R**) system to the inertial system.

$$\Gamma=\begin{bmatrix}(P_x) & (Q_x) & (R_x)\\(P_y) & (Q_y) & (R_y)\\(P_z) & (Q_z) & (R_z)\end{bmatrix}.$$

DETERMINATION OF VELOCITY

For the determination of the osculating values the velocity vector from Hansen's theory we start w the familiar Laplacian integral

$$\mathbf{R}\times\mathbf{v}+h\mathbf{r}^0+he\mathbf{P}=0,$$

where **v** is the velocity vector, $\mathbf{r}^0$ is a unit vector in direction of **r**, and $h=[a(1-e^2)]^{-\frac{1}{2}}$. Since the posit

ctor of the auxiliary satellite $\bar{\mathbf{r}}$ is in the same direction r, i.e.,

$$\mathbf{r}(t)=(1+\nu)\bar{\mathbf{r}}(z),$$

here $(1+\nu)$ is merely a lengthening or shortening ctor, then

$$\mathbf{r}^0=\bar{\mathbf{r}}^0=(\mathbf{P})\cos\bar{f}+(\mathbf{Q})\sin\bar{f}.$$

ence Eq. (16) becomes

$$\mathbf{R}\times\mathbf{v}+h(\mathbf{P})\cos\bar{f}+h(\mathbf{Q})\sin\bar{f}+he\mathbf{P}=0. \quad (17)$$

a vector cross multiplication of $\mathbf{R}=(\mathbf{R})$ into the ove equation we obtain osculating $\mathbf{v}$ in terms of '), $(\mathbf{Q})$, and $\mathbf{Q}$; namely,

$$\mathbf{v}=h(\mathbf{Q})\cos\bar{f}-h(\mathbf{P})\sin\bar{f}+he\mathbf{Q}. \quad (18)$$

his equation represents the form the Hamiltonian ntegral" takes in the Hansen theory. From Eqs. (9), 2), and (13) we find

$$he\mathbf{Q}=he_0(\mathbf{Q})+\frac{1}{2(a_0)^{\frac{1}{2}}}\{(1-e_0^2)^{\frac{1}{2}}(\mathbf{Q})Y-(\mathbf{P})Z\}. \quad (19)$$

he velocity then becomes

$$=\frac{(1-e_0^2)^{\frac{1}{2}}(\mathbf{Q})}{(a_0)^{\frac{1}{2}}}\left[\frac{\cos E}{1-e_0\cos E}\frac{h}{h_0}+\tfrac{1}{2}Y\right]$$

$$-\frac{(\mathbf{P})}{(a_0)^{\frac{1}{2}}}\left[\frac{\sin E}{1-e_0\cos E}\frac{h}{h_0}+\tfrac{1}{2}Z\right]. \quad (20)$$

onsequently, from "Application of Hansen's Theory" Musen 1959)

$$\mathbf{r}=(1+\nu)\Gamma\cdot\begin{bmatrix}a_0(\cos E-e_0)\\ a_0(1-e_0^2)^{\frac{1}{2}}\sin E\\ 0\end{bmatrix}, \quad (21)$$

d now from Eqs. (15) and (20),

$$\mathbf{v}=\frac{1}{[a_0]^{\frac{1}{2}}}\Gamma\cdot\begin{bmatrix}-\dfrac{\sin E}{1-e_0\cos E}\dfrac{h}{h_0}-\tfrac{1}{2}Z\\ \dfrac{(1-e_0^2)^{\frac{1}{2}}\cos E}{1-e_0\cos E}\dfrac{h}{h_0}+\dfrac{(1-e_0^2)^{\frac{1}{2}}}{2}Y\\ 0\end{bmatrix}. \quad (22)$$

THE OSCULATING ELEMENTS

The determination of the osculating elements is an tra result since one could obtain them from $\mathbf{r}$ and $\mathbf{v}$. owever, it is felt that the theoretical expressions for e elements in terms of the constants of integration, , e_0, and i_0 and some of the resulting series of the eory, λ_1, λ_2, λ_3, λ_4, W, h_0/h, would be useful. We obtain

$$a=\frac{a_0(1-e_0^2)}{1-\beta^2-\gamma^2}\left(\frac{h_0}{h}\right)^2$$

$$e=(\beta^2+\gamma^2)^{\frac{1}{2}}$$

$$\tan i=\frac{[(P_z)^2+(Q_z)^2]^{\frac{1}{2}}}{\lambda_4^2+\lambda_3^2-\lambda_2^2-\lambda_1^2}$$

$$\tan\omega=\frac{\beta(P_z)+\gamma(Q_z)}{\beta(Q_z)-\gamma(P_z)}$$

$$\tan\theta=\frac{(P_y)(Q_z)-(Q_y)(P_z)}{(P_x)(Q_z)-(Q_x)(P_z)}$$

$$\left(\frac{1+e}{1-e}\right)^{\frac{1}{2}}\tan\frac{E_{\text{osc}}}{2}=\frac{\left(\dfrac{1+e_0}{1-e_0}\right)^{\frac{1}{2}}\tan\dfrac{E}{2}-\dfrac{e-\beta}{\gamma}}{1+\dfrac{e-\beta}{\gamma}\left(\dfrac{1+e_0}{1-e_0}\right)^{\frac{1}{2}}\tan\dfrac{E}{2}}.$$

Finally from the osculating value of the eccentric anomaly, obtained in the equation above, we find

$$M=E_{\text{osc}}-e\sin E_{\text{osc}}.$$

We have applied the formulae derived in this paper to the Vanguard I satellite for a particular moment of time. Using a computer program coded by Mrs. Jaylee Burley, we have found that the osculating elements obtained from the position and velocity vectors are in complete agreement with those obtained from the immediately foregoing formulae.

CONCLUSION

The ability to obtain osculating elements and/or velocity from the modified Hansen theory represents a significant adjunct to that theory. Comparison with other general perturbations theories and with special perturbations techniques is now possible. Accurate transition from the general theory to numerical integration makes it possible to transfer to the latter method when additional disturbing forces, not included in the general theory, become of consequence.

ACKNOWLEDGMENT

We wish to express our appreciation to Dr. P. Musen for several valuable discussions during the course of this investigation.

REFERENCES

Hansen, P. A. 1838, *Fundamenta Nova Investigonis Orbital Verae quam Luna Perlustrat* (Carl Glaeser, Gotha).

——. 1862, *Darlegung Der Theoretischen Berechnung der in den Mondtafeln Angewandten Störungen.* (S. Hirzel, Leipzig).

Musen, P. 1959, *J. Geophys. Research* 64, 2271–2279.

An Algorithm Applicable to Numerical Integration of Orbits in Multirevolution Steps

C. J. COHEN AND E. C. HUBBARD
U. S. Naval Weapons Laboratory, Dahlgren, Virginia
(Received June 21, 1960)

In the numerical integration for orbits, it has been proposed that the secular variation of the orbit elements be computed in multirevolution steps. The present paper develops an algorithm for a k-revolution step which is analogous to the algorithm for a step of integration by Adams' method. The analogue of the derivative generated at each integration step by Adams' method is the increment to the orbit elements for one revolution generated at each k-revolution step. The coefficients in Adams' integration formula are replaced by polynomials in $1/k$. These polynomials are the same as those appearing as coefficients in Lubbock's summation formula and the constants in these polynomials are the Adams coefficients.

1. INTRODUCTION

IN the numerical integration of differential equations governing orbital motion it has been proposed (Taratynova 1957; Thomas 1958) that the change in the orbit elements for one revolution be determined by conventional numerical integration over one revolution and that this secular change in turn serve as the basis for a multirevolution integration step. Taratynova treats the secular change for one revolution as a derivative with respect to revolution number and then numerically integrates with respect to revolution number. Our method, while similar to that of Taratynova, treats the secular change for one revolution as a finite difference, and introduces a new Adams-type corrector formula which reduces to Adams' formula only in a limiting case. The same refinement to the Taratynova method has been independently developed by Mace and Thomas (1960) and numerically verified by them. In their study, they applied a multirevolution predictor formula to the first and second sums of the acceleration components, rather than a corrector formula to the orbit elements. Our work further supplements theirs through the development of a general formula [Eq. (15)] for the coefficients in the formula for the multirevolution increment, which we evaluate and present through the tenth difference terms.

Our multirevolution step is started by extrapolating the orbit elements k revolutions ahead. Then, starting with these extrapolated values, the differential equations of motion are numerically integrated over one revolution. This integration yields the increment to the orbit elements for one revolution at the end of the k-revolution step. The extrapolated values of the orbit elements are then improved by use of our corrector formula, which is in terms of this increment for one revolution and its backward differences with respect to the k-revolution spacing. As in Adams' method, the corrector formula may also be applied to an extrapolated difference table to obtain the extrapolated orbit elements required at the beginning of the step. In the next section the corrector formula is derived. In the final section the growth of roundoff error discussed.

2. DERIVATION OF CORRECTOR FORMULA

Let y_n be an orbit element evaluated at the end the nth revolution; let the increment for one revolu be

$$f_n = y_{n+1} - y_n,$$

and let the backward differences with respect to k-revolution spacing be defined by

$$\nabla f_n = f_n - f_{n-k}, \quad n = k, 2k, 3k, \cdots.$$

Further let factorial polynomials be defined by

$$x^{(\pm n)} = \prod_{r=0}^{n-1} (x \mp r).$$

By the Newton-Gregory formula for interpola using backward differences,

$$f_{k-i} = \sum_{j=0} \frac{1}{j!} \left(\frac{-i}{k}\right)^{(-j)} \nabla^j f_k$$

$$= \sum_{j=0} \frac{(-)^j}{j!} \left(\frac{i}{k}\right)^{(j)} \nabla^j f_k.$$

Summing on i yields the k-revolution increment in orbit element

$$y_k - y_0 = \sum_{i=1}^{k} f_{k-i}$$

$$= \sum_{j=0} \frac{(-)^j}{j!} \sum_{i=1}^{k} \left(\frac{i}{k}\right)^{(j)} \nabla^j f_k$$

$$= k \sum_{j=0} \lambda_j \nabla^j f_k.$$

We now wish to develop further the formula for coefficients λ. One has

$$\lambda_0 = 1$$

$$\lambda_1 = -\tfrac{1}{2}[1 + (1/k)]$$

$$\lambda_j=\frac{(-)^j}{j!k}\sum_{i=1}^{k}\left(\frac{i}{k}\right)^{(j)} \quad \text{for} \quad j>1. \tag{8}$$

e factorial polynomial in Eq. (8) may be expanded o a power series

$$\left(\frac{i}{k}\right)^{(j)}=\sum_{r=1}^{j}S_j^r\left(\frac{i}{k}\right)^r, \tag{9}$$

ere S_j^r is the Stirling number of the first kind rdan 1939a). These numbers satisfy the recurrence ation

$$S_j^{r+1}=S_j^{r-1}-jS_j^r \tag{10}$$

rting from

$$S_0^0=1, \tag{11}$$

d

$$S_r^0=S_0^r=0 \quad \text{for} \quad r>0. \tag{12}$$

Next, in Eq. (8) after substituting from Eq. (9), sum on i may be expanded into a power series in k Bernoulli's formula (Jordan 1939b).

$$\frac{1}{k}\sum_{i=1}^{k}\left(\frac{i}{k}\right)^r=\frac{1}{r+1}\sum_{q=0}^{r/2}\binom{r+1}{2q}\frac{B_{2q}}{k^{2q}}+\frac{1}{2k}, \quad r>0. \tag{13}$$

re the sum on q is to the greatest integer in $r/2$ and Bernoulli numbers B_{2q} are those beginning

$$(B_0, B_2, B_4,\cdots)=(1, 1/6, -1/30,\cdots). \tag{14}$$

Upon expanding Eq. (8) into a power series, first in by Eq. (9) and then in $1/k$ by Eq. (13), one finds

$$\lambda_j=\frac{(-)^j}{j!}\sum_{q=0}^{j/2}\left[B_{2q}\sum_{r=2q}^{j}\frac{S_j^r}{r+1}\binom{r+1}{2q}\right]\frac{1}{k^{2q}}, \quad j>1. \tag{15}$$

re the $1/k$ term to be expected from Eq. (13) does appear because it contains

$$\sum_{r=1}^{j}S_j^r=0, \quad j>1, \tag{16}$$

a factor.

The λ's through λ_{10} are thus found, by Eqs. (6), (7) l (15), to be the following polynomials in $1/k$.

$$=1 \tag{17}$$

$$=-\frac{1}{2}\left(1+\frac{1}{k}\right) \tag{18}$$

$$=-\frac{2}{4!}\left(1-\frac{1}{k^2}\right) \tag{19}$$

$$=-\frac{1}{4!}\left(1-\frac{1}{k^2}\right) \tag{20}$$

$$\lambda_4=-\frac{1}{6!}\left(1-\frac{1}{k^2}\right)\left(19-\frac{1}{k^2}\right) \tag{21}$$

$$\lambda_5=-\frac{3}{2(6!)}\left(1-\frac{1}{k^2}\right)\left(9-\frac{1}{k^2}\right) \tag{22}$$

$$\lambda_6=-\frac{2}{3(8!)}\left(1-\frac{1}{k^2}\right)\left(863-\frac{145}{k^2}+\frac{2}{k^4}\right) \tag{23}$$

$$\lambda_7=-\frac{5}{3(8!)}\left(1-\frac{1}{k^2}\right)\left(11-\frac{2}{k^2}\right)\left(25-\frac{1}{k^2}\right) \tag{24}$$

$$\lambda_8=-\frac{1}{10!}\left(1-\frac{1}{k^2}\right)\left(33\,953-\frac{9247}{k^2}+\frac{497}{k^4}-\frac{3}{k^6}\right) \tag{25}$$

$$\lambda_9=-\frac{7}{2(10!)}\left(1-\frac{1}{k^2}\right)\left(8183-\frac{2617}{k^2}+\frac{197}{k^4}-\frac{3}{k^6}\right) \tag{26}$$

$$\lambda_{10}=-\frac{1}{12!}\left(1-\frac{1}{k^2}\right)\left(3\,250\,433-\frac{1\,184\,767}{k^2}+\frac{114\,597}{k^4}-\frac{2993}{k^6}+\frac{10}{k^8}\right). \tag{27}$$

3. RELATIONS TO OTHER FORMULAE

Equation (5) is related to Lubbock's summation formula, the coefficients λ_j being essentially the same in both formulae (Steffensen 1927). The Lubbock formula, however, is more complicated and moreover would not serve our purpose.

The interval defining f in Eq. (5) is an orbit revolution only in our particular application. Actually Eq. (5) is a valid solution for more general systems of difference equations, and the interval h defining f may be arbitrarily chosen. As h approaches zero with hk held fixed, the limit of Eq. (5) is the increment to y expressed in terms of differences of its derivative. The limit is, therefore, the Adams corrector formula. One finds, upon multiplying the right member of Eq. (5) by h/h

$$y(hk)-y(0)=\lim_{\substack{h\to 0\\ hk \text{ fixed}}}\sum_{j=0}hk\lambda_j\left(\nabla^j\frac{f}{h}\right)_{x=hk} \tag{28}$$

$$=hk\sum_{j=0}(\lim_{k\to\infty}\lambda_j)\nabla^j\left(\frac{dy}{dx}\right)_{x=hk}.$$

Thus

$$\lim_{k\to\infty}\lambda_j=\frac{(-)^j}{j!}\sum_{r=0}^{j}\frac{S_j^r}{r+1} \tag{29}$$

are the Adams coefficients. From inspection of Eqs. (17)–(27) the limit as k approaches infinity may indeed be recognized as the Adams coefficients.

The foregoing is an analytic presentation of multistep

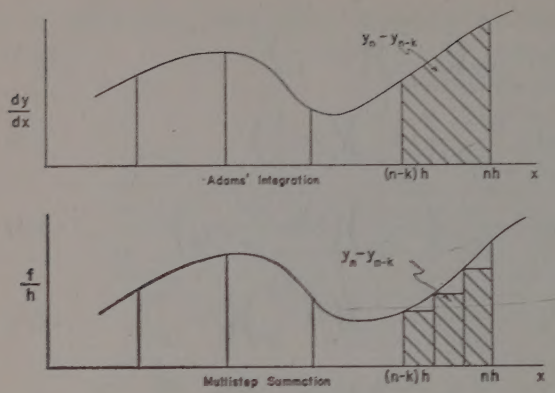

FIG. 1. Comparison of Adams' integration with multistep summation.

summation and its relation to Adams' integration. The corresponding geometry is shown in Fig. 1. In the Adams part of the figure the curve is a polynomial fitted to dy/dx at intervals kh, and the shaded area is

$$\int_{(n-k)h}^{nh} \left(\frac{dy}{dx}\right) dx = y_n - y_{n-k}. \tag{30}$$

In the multistep part of the figure, the curve is a polynomial fitted to f/h at intervals kh $(k=3)$ and the shaded area is

$$\sum_{i=1}^{k} \left(\frac{f_{n-i}}{h}\right) h = y_n - y_{n-k}. \tag{31}$$

If kh is held fixed but k approaches infinity, f/h approaches dy/dx and it is apparent from the figure also that multistep summation reduces to Adams integration.

4. ACCUMULATION OF ROUNDOFF ERROR

In the multi-interval stepping, the growth of rou off errors can be adverse. In one multi-interval st one has

$$\nabla y \simeq kf, \tag{}$$

and, taking variances,

$$\sigma_{\nabla y}^2 \simeq k^2 \sigma_f^2. \tag{}$$

On the other hand, by k single-interval steps, one

$$\nabla y \simeq \sum_{i=0}^{k-1} f_i. \tag{}$$

Assuming that each f_i has roughly the same varia and neglecting the correlation of the roundoff er in successive f's,

$$\sigma_{\nabla y}^2 \simeq k \sigma_f^2, \tag{}$$

which is less than the variance in the multi-interval st for fixed variance of f. The variance of f can, howe be considerably reduced by summing the increments the orbit elements during the numerical integrat over one revolution rather than by differencing orbit elements as implied by Eq. (1). The roun error of f thus becomes a small fraction of the variat of y over a revolution rather than the same fraction o

REFERENCES

Jordan, C. 1939a, *Calculus of Finite Differences* (Budapest), p.
——. 1939b, *ibid.* p. 246.
Mace, D., and Thomas, L. H. 1960, *Astron. J.* **65**, 300.
Steffensen, J. F. 1927, *Interpolation* (Williams & Wilkins C pany, Baltimore), p. 139.
Taratynova, G. P. 1957, article in *Uspekhi Fizicheskikh Nauk* translated in *The Russian Literature of Satellites*, Part I (In national Physical Index, Inc., New York, 1958), pp. 71–85 "The Motion of an Artificial Earth Satellite···."
Thomas, L. H. 1958, *Astron. J.* **63**, 459.

Dust and Gas in Globular Clusters*

MORTON S. ROBERTS†
Department of Astronomy, University of California, Berkeley, California
(Received July 18, 1960)

The possibility that dust and gas may exist in a significant ount in globular clusters is considered. It is shown that the y method of detecting such intraglobular matter at present is its obscuring effects, especially if the material has collected clouds within the cluster. Evidence is presented that such ids exist in globular clusters, appearing as dark regions and es in the cluster. It is found that statistical fluctuations in the jected stellar distribution of the cluster cannot account for se dark regions. If these obscuring effects are attributed to eground clouds we must expect at least twenty such clouds square degree of sky at high galactic latitudes. It is concluded t such an explanation cannot account for all the obscured ions that have been found in globular clusters.

The source of the intraglobular clouds can be satisfactorily accounted for by the mass shed by stars evolving to the white-dwarf stage. About 0.5% of the total mass of the cluster becomes available in this manner in the time between passages of the cluster through the galactic plane.

The effects of such intraglobular matter on the stellar population of the cluster are discussed. Such clouds may condense into stars and thus account for those stars which lie in the vicinity of the main sequence and above the turnoff point in the color-magnitude diagrams of some globular clusters. These stars appear to have a nonrandom distribution in the cluster, supporting the above suggestion as to their origin.

I. INTRODUCTION

GLOBULAR clusters are thought to be free of interstellar dust and gas. It is important to amine this conclusion critically because of the nificant position ascribed to globular clusters in our rent evolutionary concepts. Such a consideration ms the subject matter of the present paper. It will shown that interstellar matter may indeed exist in bular clusters; the observational evidence leading this conclusion is presented in Sec. II. A possible rce of intraglobular matter and processes which id to remove such matter from clusters are discussed Sec. III. The effects of intraglobular material on stellar population of a cluster together with idence that such effects may exist are presented in c. IV. A summary is given in the last section.

II. OBSERVATIONAL DATA

Interstellar matter may be detected by two general thods: by its obscuring effects and, under the proper nditions, by its emission characteristics. The appli-ion of these methods to globular clusters is considered the present section.

(a) Obscuring Matter

Evidence that dark lanes and regions exist in bular clusters is at least 100 years old, dating back the Earle of Rosse's (1861) visual observations of 13. He published a remarkable sketch showing a ies of dark lanes within the cluster. Interest in this oblem was renewed about the turn of the century Holden (1891) who, using photographic methods, o called attention to the dark lanes in M13. An interesting summary of these and other similar observations is given by Miss Clerke (1903).

More recent observations of obscured regions in globular clusters are those of FitzGerald (1955) who comments on some dark lanes in ω Centauri, and those of Idlis and Nikolsky (1959) who discuss M4. In the latter case the authors consider the possibility of statistical fluctuations in the projected stellar distribution of the cluster as a possible explanation of the dark regions in M4. They find that it is highly unlikely that such fluctuations would account for the size and number of such lanes and conclude that there is obscuring matter in the cluster.

Mrs. Hogg (1959a,b) has also drawn attention to the dark regions in globular clusters. She, however, suggests that these obscuring effects may be due to (presumably close) foreground clouds, pointing out that globular clusters present an ideal background against which such clouds would be detected.

To examine this problem in more detail all globular clusters with galactic latitude $\geq 15°$ and lying within the declination range of the Palomar Sky Survey ($\delta > -27°$) were examined. Two sources were used, the Sky Survey prints and the Lick-Crossley plate file. These sources complement each other; the Crossley plates with their greater scale and brighter limiting magnitude allow an examination of the more central region of the cluster whereas the Survey prints, reaching a fainter limiting magnitude, yield information on the outer region of the cluster.

Although factors such as image growth, exposure, and cluster concentration class affect general appearance of a cluster, it is possible to identify regions in a number of clusters which have a high likelihood of being caused by obscuration. Thirty-two globular clusters lie within the specified declination and galactic latitude limits. At least 12 of these clusters show one or more prominent dark regions and lanes on either or both the Crossley plates and Sky Survey prints. These

* This work was supported in part by the United States Force.
† National Science Foundation Postdoctoral Fellow, 1958–1959. sent address: Harvard College Observatory, Cambridge, ssachusetts.

TABLE I. Globular clusters containing dark regions and lanes.

NGC	*M*	NGC	*M*	NGC	*M*
1904	79	5904	5	6341	92
2419		6171		6402	14
5024	53	6205	13	6864	75
5272	3	6254	10	7078	15

clusters are listed in Table I and several are illustrated in Figs. 1 and 2.

The 32 clusters examined in this survey cover 0.8 square degree of sky. This figure is based on Mowbray's (1946) estimates of their diameters. If all the regions designated as obscured are to be attributed to foreground clouds and not to intraglobular matter or statistical fluctuations in the distribution of stars within the cluster, then the number of such foreground clouds per square degree of sky, and at the higher galactic latitudes considered here, will be $1.25N$, where N is the number of obscured regions identified in the 32 clusters studied. A lower limit for N is 16. We would therefore expect at least 20 interstellar clouds per square degree of sky. Because their appearance is so pronounced, these clouds must be of rather high opacity. Neglecting for the moment the question of statistical fluctuations, we are forced to accept either of two conclusions: (1) Relatively opaque interstellar clouds at high galactic latitudes are much more common than heretofore thought, or (2) globular clusters contain interstellar clouds.

On the basis of their general appearance and opacity, we may compare the foreground clouds proposed in (1) to globules. An extensive study of the frequency and distribution of globules has not been made. The preliminary survey of selected areas in the region of the Milky Way by Bok and Reilly (1947) will, however, serve as an adequate basis for comparison. By searching in areas of background nebulosity or high star density they concluded that globules "seem to occur at the rate of one per square degree." At least twenty times this number is needed to account for the obscured regions found in globular clusters. This large difference makes (1), above, unlikely. Further, such a high projected density of foreground clouds would predict obscuration in at least some elliptical nebulae. This is not the case. Galaxies such as NGC 205 and NGC 5128 (radio source 13S4A) which are classified as peculiar cannot owe their peculiar appearance to foreground clouds; the unusual features are obviously associated with the galaxy itself.

The obscured regions are prominent in photographs taken over a wide range of exposure time. A significant feature in the longer exposed photographs is the frequent appearance of stars superposed on an obscured region. It should be noted that even with the appearance of these stars in obscured regions there often remains a significantly large area where there is a striking absence of stars. From star counts in the general field, it is immediately evident that these sta cannot be field stars in front of a noncluster obscurin cloud; the number of stars per square degree of sky far too low. It has been suggested (Hogg 1959a) that th appearance of these stars represent cluster stars shinin through a nearby foreground cloud, such stars becomin more visible with longer exposure. For such a situatio one would require a large fluctuation of opacity in th nearby small obscuring clouds. In addition there woul have to be a cluster star, of sufficient brightness to b visible, located in exactly the same line of sight as th low-opacity region of the nearby foreground clou Such a set of circumstances seems very unlikely. would be more reasonable to expect that longe exposures would bring up faint cluster stars which a situated in front of an obscured region located *withi* the cluster.

Thus, if we are to attribute the obscured regions t foreground clouds we require:

(i) The occurrence of such clouds to be twent times greater than that of globules in the galactic plan

(ii) An explanation of their absence as seen again other bright backgrounds such as elliptical nebulae.

(iii) Large fluctuations in the opacity of such cloud so that we may see cluster stars through the clouds.

Or, we may attribute the obscured regions to intra globular clouds. Since the necessary mass for suc clouds can easily be accounted for, in fact is expecte (Sec. III), we find it reasonable to conclude tha interstellar matter, concentrated into clouds, exists globular clusters.

(b) Statistical Fluctuations

In the preceding discussion it was assumed that th obscured regions were not caused by statistic fluctuations in the projected stellar distribution of cluster. We will now proceed to show that such a assumption is reasonable, i.e., that, on the basis statistical fluctuations in the stellar distribution, th probability of finding as large a star-free area, and close to the cluster center as the obscured regions, vanishingly small.

The most direct approach to such a problem is t construct a two-dimensional model of a globular cluste containing the various parameters which describe cluster and see if relatively large areas are free stars. In theory an infinite or at least a very larg number of such models would have to be constructe before some definite statement as to the probabilit of finding large star-free regions could be mad However, there is another approach which may b used. In this case only one cluster model (or even pa of a model) need be constructed. From this model w may obtain the frequency distribution of differe sized star-free regions. Such a distribution may b expected to approximate a normal distribution (fo positive values only). From the sample data we ma

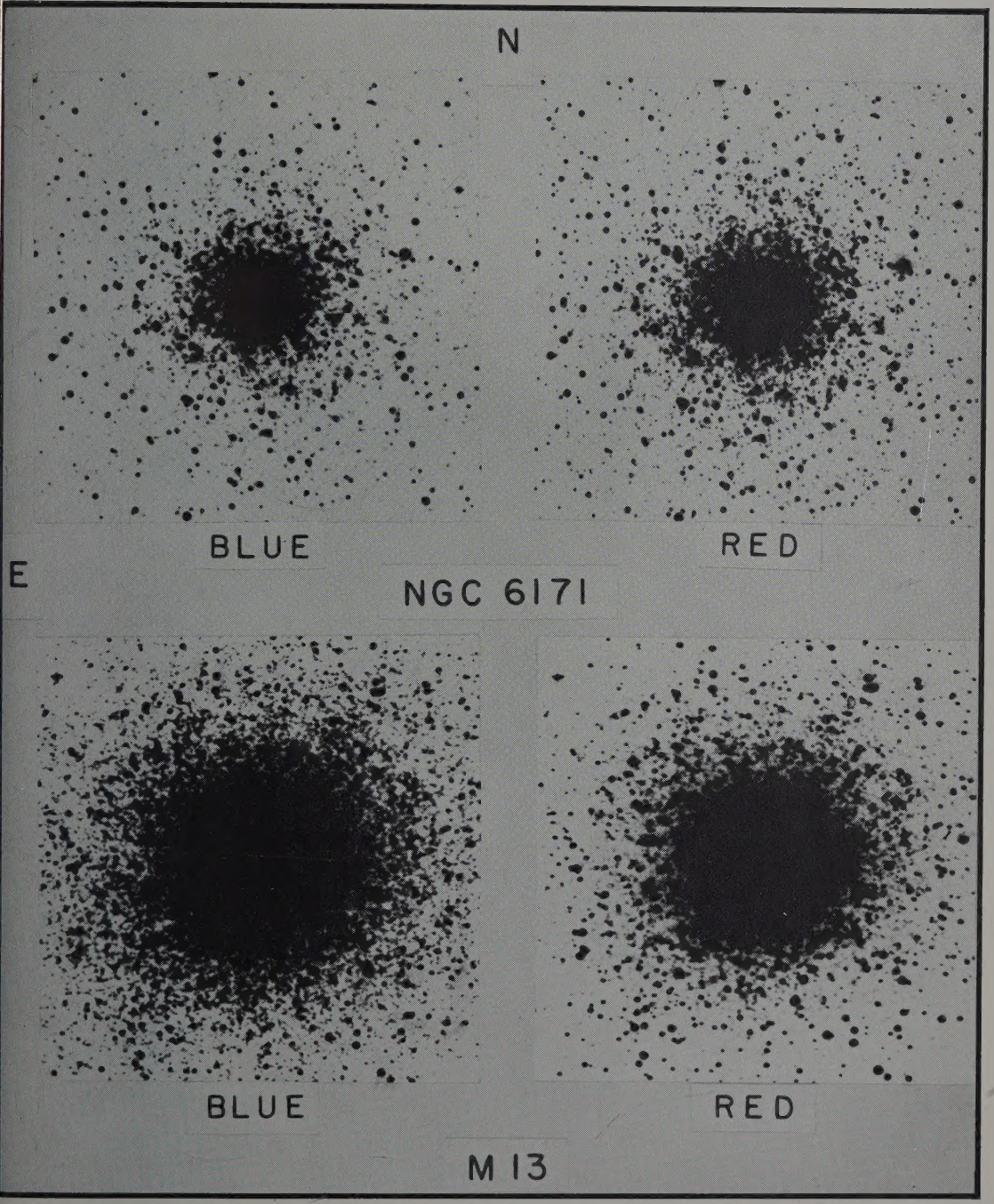

FIG. 1. Examples of globular clusters showing obscured regions near the outer part of the cluster. NGC 6171 was photographed th the 48-inch Schmidt (Copyright National Geographic Society—Palomar Observatory Sky Survey). The M13 photographs were ken with the Crossley Reflector, the blue by N. U. Mayall, the red by A. G. Mowbray. Note particularly the regions at position gles 5° and 210° in NGC 6171 and at 130° in M13.

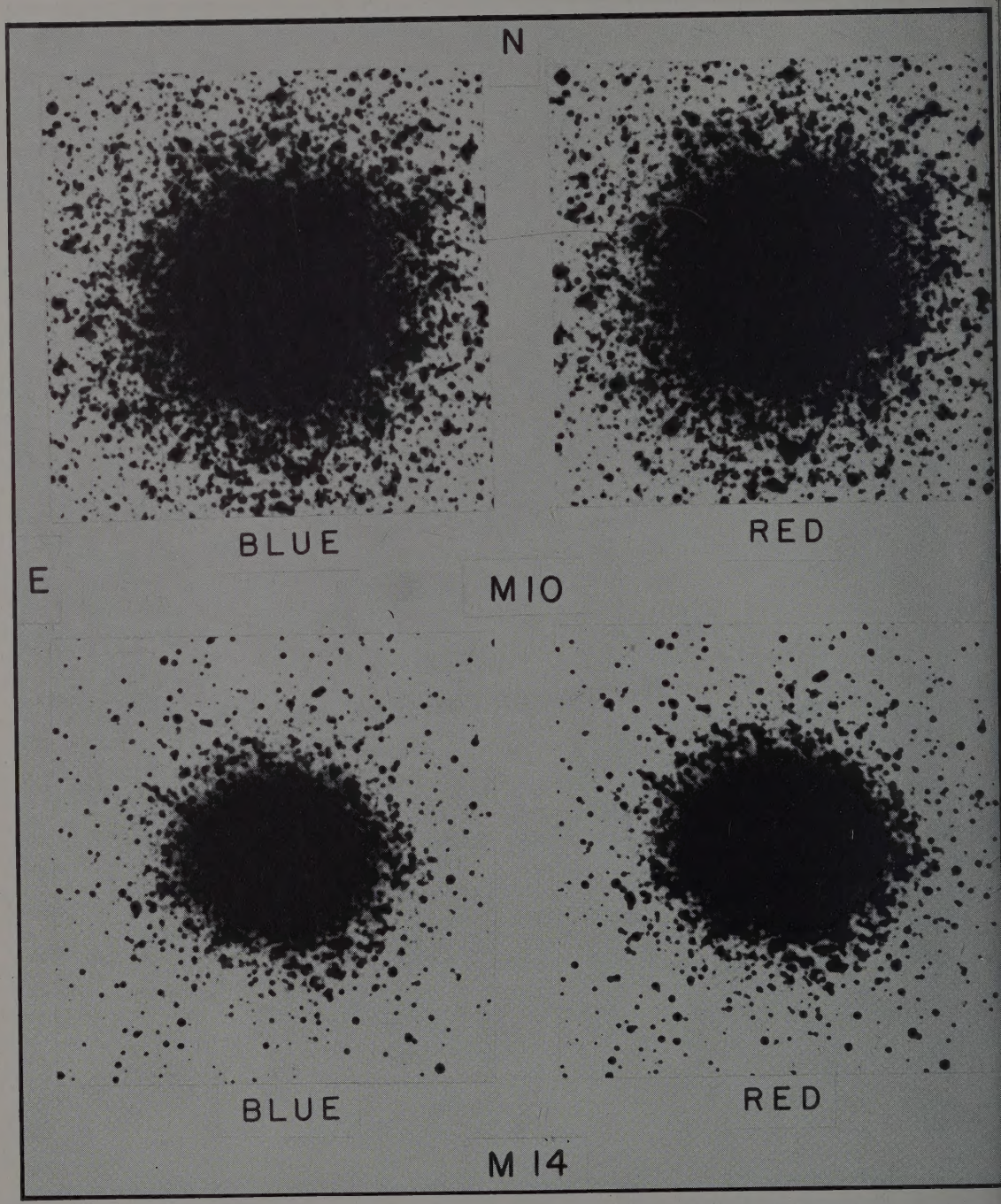

FIG. 2. Examples of globular clusters showing obscured regions near the outer part of the cluster. Both clusters were photograph with the 48-inch Schmidt (Copyright National Geographic Society—Palomar Observatory Sky Survey). Note particularly the regi at position angle 0° in M10 and 215° in M14.

ıen evaluate the dispersion of this distribution and ıus assign a probability to the finding of any sized ar-free area. It is this second method which was nployed here.

The following information is necessary for the ɔnstruction of a globular cluster model:

(1) The projected stellar density gradient, $N(R)$.
(2) The cluster luminosity function, $\varphi(M)$.
(3) The limiting magnitude, m_l, of the model.
(4) The relation between image size, d, and apparent agnitude, m.

model patterned after M13 was constructed using ıe following input data. Shapley's (1915) star counts the cluster gave $N(R,m)\Delta R\Delta m$, the number of ars brighter than magnitude m in Δm and within ɔncentric annuli of size $R\pm\Delta R$. A cluster luminosity ınction (M3, Sandage 1957) allowed extrapolation om Shapley's magnitude limit to $m_l\simeq 18.5$ (photo-aphic). The Greenwich formula

$$m=a+bd^{\frac{1}{2}}$$

as used to relate image diameter, d, to apparent agnitude; this approximate relation is adequate for ıe present purpose. The constants a and b were ɛrived from measures on Mt. Wilson 60″ photographs M13. From these data a table of $N(R\pm\Delta R, m\pm\Delta m)$ its equivalent $N(R\pm\Delta R, d\pm\Delta d)$ was constructed. random number drawn from Triplett's table (1952) ıd representing the polar coordinates of an individual ar was then assigned to each of the N stars. The sulting model for two quadrants of the annulus $\leq R<2'$ is shown in Fig. 3.

The frequency of different sized star-free regions in is model is shown by the histogram in Fig. 4. The ıta are sufficiently well represented by a normal stribution with a standard deviation $\sigma=61$; the fit is own in the figure. This particular annular region for 13 was chosen because it contains a very prominent ırk lane visible at position angle 130° in Fig. 1. The ea of the lane in a photograph of the above limiting agnitude is about 460 square seconds of arc; it is own as an X in the frequency distribution of Fig. 4. ı the basis of this model, this obscured region is rger than 7σ; the probability of finding such a large

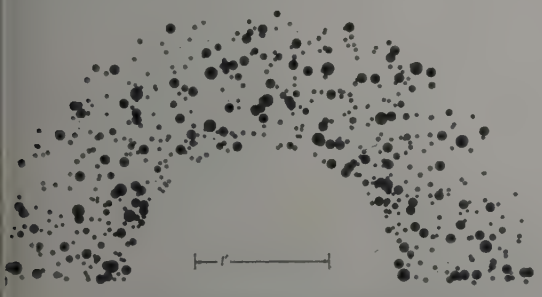

FIG. 3. Model globular cluster. One-half of the annulus $1'\leq R<2'$ is shown.

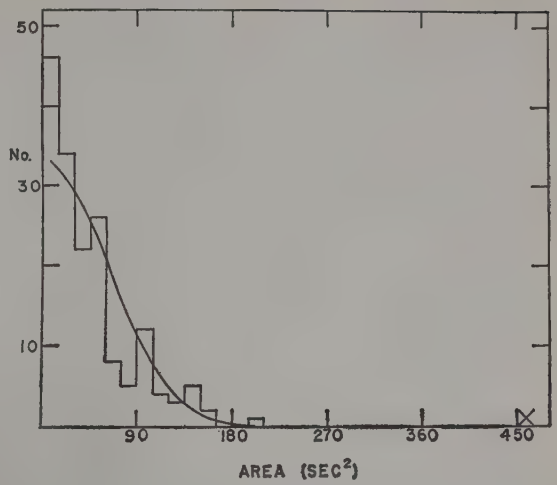

FIG. 4. Frequency distribution of different sized star-free regions in the model globular cluster. A normal curve with $\sigma=61$ is fitted to the histogram. The X represents the size of the obscured region in M13.

lane strictly on the basis of statistical fluctuation is essentially zero. Several of the obscured regions in the clusters listed in Table I are comparable in size to the M13 lane and a similar conclusion may be drawn as to their reality.

It should be pointed out that a cluster model constructed in the preceding fashion *overestimates* the sizes of star-free regions. This results from a failure in the model to account for the turbidity effect in the photographic emulsion. For the highly crowded stars in a globular cluster this overestimation may be quite large. This lends further support to the conclusion that the more centrally located regions in globular clusters which are being considered here are *not* due to statistical fluctuations of the stellar distribution.

In summary we may say that the dark lanes and regions in globular clusters are very likely real; i.e., they are not due to statistical fluctuations. They may be due to the obscuring effects of nearby clouds, but on the basis of their frequency and of the appearance of "foreground" stars it is more likely that these clouds are actually located within the cluster. The lack of a mechanism by which such clouds might form cannot be used as an argument against their existence, for then we face a similar problem as regards the interstellar clouds in the general field.

(c) Mass of Intraglobular Clouds

We may assign a lower limit to the mass of an intraglobular cloud from knowledge of its dimensions and opacity by assuming that the observed obscuring effects of the cloud are produced wholly by dust particles of optimum size for scattering and absorption. Adopting the values employed by Bok (1948) in assigning masses to globules we obtain

$$A_{pg}=6.7\times 10^{25}\delta, \qquad (1)$$

where A_{pg} is the absorption for photographic light in magnitudes per kiloparsec and δ is the dust-particle density in g/cm³. We will use as input data values derived for the dark nebula in M13; these values are representative of the obscured regions in a number of globular clusters. The total photographic absorption is at least five magnitudes; a conservative estimate of the size of the projected image of the cloud is ~ 1 pc$\times 3$ pc. We will assume that the cloud is a cylinder seen perpendicular to its major axis. The cloud is more likely to be spherical, the observed elongated form being caused by images of neighboring and foreground bright stars. We will thus underestimate the total mass of the cloud by assuming that it is a cylinder of the above dimensions.

The resultant dust-particle density is $\delta = 7.5 \times 10^{-23}$ g/cm³ and the total mass of the dust particles $\mathfrak{M}_{\text{dust}}/\mathfrak{M}_\odot > 2.6$. Adopting $\mathfrak{M}_{HI}/\mathfrak{M}_{\text{dust}} = 10^2$, we obtain $\mathfrak{M}_{\text{cloud}}/\mathfrak{M}_\odot > 260$. There may be several clouds in a cluster; only those lying in that part of the cluster closest to the sun would be detectable; the total mass of interstellar matter within a globular cluster would then be proportionally higher. A value of $\sim 10^3 \mathfrak{M}_\odot$ would be a reasonable estimate of the total mass of interstellar matter in a globular cluster.

(d) Emission from Possible *H*I and *H*II Regions in Globular Clusters

We have assumed in the above calculation that most of the intraglobular matter is hydrogen. If this hydrogen is neutral and atomic it should be detectable by its 21-cm radiation. A search for such radiation from the globular clusters M3 and M13 was made with the 85-foot radio telescope of the National Radio Astronomy Observatory (Roberts 1959). A conservative upper limit (i.e., it may be well below this limit) to the antenna temperature for both of these clusters is 0.4°K. For small optical depths, τ, this antenna temperature yields upper limits to the mass of *H*I; for M3 it is $700 \mathfrak{M}_\odot$ and for M13, $200 \mathfrak{M}_\odot$.

These results must be viewed with caution. Although they are based on an observational upper limit to the antenna temperature, they are also dependent upon the assumed opacity.

The assumption of small τ for such clouds may be incorrect; this together with an expected low value of the *H*I kinetic temperature in a globular cluster would result in an underestimation of the amount of *H*I present. Further, a significant amount of hydrogen in a molecular form may be present in the obscured regions of globular clusters and would thus be undetectable. The formation of molecular hydrogen would be favored in the highly opaque and presumably cool regions considered here.

Our current lack of knowledge of the opacity, gas kinetic temperature, and the ratio of atomic to molecular hydrogen make an interpretation of the above 21-cm antenna temperature uncertain.

Globular clusters are known to contain stars whi have relatively high surface temperatures; these a the stars on the blue part of the color-magnitu horizontal branch. These stars may be expected form significant *H*II regions when surrounded interstellar matter. A characteristic emission line fr such *H*II regions is λ3727. This line has not be observed in the integrated spectra of globular clust (Mayall 1946). It therefore is important to compu the expected intensity of this line to see if its absen is consistent with the concept of intraglobular matt

Minkowski and Osterbrock (1959) have consider a similar problem, the occurrence of λ3727 in t spectra of some elliptical nebulae. Lacking data individual exciting stars in these nebulae they assum that the relative frequency of such stars is the same in globular clusters. They then computed the expect intensity of λ3727 for the globular cluster M3, for whi the necessary data were available and applied th result to their discussion of E nebulae. Their resu will be adopted here, but with an important modific tion which will be noted below.

We wish to compute the total expected emission λ3727 in ergs/sec and compare this value to the ener contained in a corresponding wavelength region in t continuous spectrum of a globular cluster. Minkows and Osterbrock have evaluated the emission c efficient $j_{\lambda 3727}$ in ergs/sec cm³, for an *H*II region wi an electron temperature of 10 000°K and an electr density less than 10^3/cm³; they obtained $j_{\lambda 3727} = 1.$ $\times 10^{-25} N_H^2$ ergs/sec cm³, where N_H is the density hydrogen ions or atoms per cubic centimeter. Th have also computed the ionizing radius for the cluster stars which would make a significant contrib tion to the ionized volume which, with the clust luminosity function, yields the total ionized volum This together with $j_{\lambda 3727}$ gives the total energy emitt per second in λ3727.

Implicit in these calculations is the assumption th the interstellar matter is *uniformly* distributed throug out the cluster. Only then would the full ionizi effect of each star contribute to the total λ3727 emissio We have seen, however, that intraglobular matter m be primarily concentrated in clouds. For such situation the ionizing effect of an exciting star situat at some distance from the cloud will be reduced by factor proportional to the square of the distan between star and cloud (Strömgren 1948). Specifical if S is the ionizing radius for the case of a star locat *in* the cloud, then for a star at a distance r from t cloud (r large compared to the dimensions of the clou the extent of ionization within the cloud R is given

$$R = S^3/3r^2. \quad ($$

Minkowski and Osterbrock tabulate individu values for $S^3 N_H^2$ for each star which will make significant contribution to the total ionized volum The sum of these values (corrected for incompletene

the cluster area studied) is $\Sigma S^2 N_H^2 = 4.5 \times 10^5$. We ill adopt this value of $\Sigma S^2 N_H^2$ as a measure of the nizing effect due to *one* star at a distance r from one loud. In general this will overestimate the emission om HII regions. The product, $E_{\lambda 3727}$ of the volume of ne ionized region and $j_{\lambda 3727}$ is $8.1 \times 10^{45}/r^6 N_H^4$ ergs/sec; ne ionized volume is assumed to be a sphere of radius 2. $E_{\lambda 3727}$ is evaluated for various values of r and N_H Table II. Only those entries for which $r >$ cloud adius are tabulated.

These values of $E_{\lambda 3727}$ are to be compared to the xpected continuous emission from the cluster in this avelength region. For this we will again make use f the calculations of Minkowski and Osterbrock. They nd that the energy emitted by M3 near λ5540 is $j_{5540} = 1.7 \times 10^{35}$ ergs/sec A. From the relative energy istribution of globular clusters (Roberts 1956) as erived from the six-color observations of Stebbins and Whitford (Stebbins 1950), we find $E_{\lambda 3727}/E_{\lambda 5540} = 0.63$; ence the energy emitted in the continuous spectrum ear λ3727 is 1.1×10^{35} ergs/sec A. Comparing this alue with those of Table II we find that only if the loud ion density is very low or the exciting star very lose to the cloud would we expect to detect λ3727 in mission. From the very high opacity of the cloud we ould expect $N_H \gg 10$. We conclude that λ3727 would ot be observable in the spectra of globular clusters. similar calculation for $H\alpha$ emission from HII regions globular clusters yields the same conclusion.

III. FORMATION AND REMOVAL OF INTRAGLOBULAR MATTER

The source of intraglobular matter must be the luster itself. The high velocity of globular clusters elative to interstellar clouds makes it virtually npossible for a cluster as a whole to pick up inter- ellar matter by an accretion process. However, there reason to expect a significant source of intraglobular atter from those cluster stars which are evolving to e white-dwarf stage and which, in the process, shed art of their mass. These considerations have pre- iously been discussed by Takebe and Matsunami 1957) and by Sandage (1957). The latter author has timated the total amount of matter which has been jected into intraglobular space in the lifetime of the uster. He obtains a value of $\sim 10^5 \mathfrak{M}_\odot$ for M3, which about one-half the present mass of the cluster. This aterial is not expected to remain in the cluster. assages by the cluster through the galactic plane will e very effective in removing the intraglobular matter.

TABLE II. Emission of λ3727 in ergs/sec for various values of r and N_H.

r_{pc} \ N_H/cm³	10	10^2	5×10^2
3			1.7×10^{32}
5		5.0×10^{33}	8.2×10^{30}
10	8.0×10^{35}	8.0×10^{31}	1.3×10^{29}

If globular clusters follow highly eccentric orbits about the galactic center (von Hoerner 1955), then M3 will spend about 4×10^8 years away from the galactic plane; most of this time the cluster will be close to apogalacticon. The average amount of interstellar matter in M3 is then

$$\frac{1}{2} \times \frac{10^5 \times 4 \times 10^8}{10^{10}} = 2 \times 10^3 \mathfrak{M}_\odot, \tag{3}$$

where the age of the cluster is taken as 10^{10} years.

The value found in Eq. (3) represents a time average over the life of the cluster. The amount of interstellar matter to be expected in a globular cluster for a recent epoch is given by

$$\Delta N \times (\Delta \mathfrak{M}/\Delta t) \times \tfrac{1}{2} T, \tag{4}$$

where ΔN is the total number of cluster stars which lie in a particular part of the color-magnitude diagram, $\Delta \mathfrak{M}$ is the mass loss suffered by these stars during their evolution, and Δt is the time necessary for a star to evolve through the particular region being considered. T is the time between passages through the galactic plane. For that part of the color-magnitude diagram which lies above the main-sequence turnoff point $\Delta N \propto \Delta t$ or $\Delta N/\Delta t$ is constant. We may therefore evaluate Δt for any convenient region of the C-M diagram, thus

$$\Delta t = 6.2 \times 10^{18} X \mathfrak{M} \int_{q_1(1)}^{q_2(2)} \frac{dq_1}{L}, \tag{5}$$

where X is the mass fraction of hydrogen in the star, L its luminosity and q_1 is the fraction of the total stellar mass located in the core (Hoyle and Schwarzschild 1955). The integral may be numerically evaluated from the model sequence computed by Hoyle and Schwarzschild (1955, Table 8) for type II stars. Such an integration yields $\Delta t \approx 6 \times 10^8$ years for the range $M_v \approx +2.4$ to $M_v \approx -3.0$. From the luminosity function for M3 (Sandage 1957) we estimate ΔN, the number of cluster stars which lie in this magnitude range and along the giant branch, as 3×10^3.

We now require only $\Delta \mathfrak{M}$. For the initial mass we adopt $1.2 \mathfrak{M}_\odot$. The final mass will be that of a white dwarf. It does not matter if the final mass over the range considered here is actually that of a white dwarf, since for some Δt this mass loss will be realized and we then make use of the relationship $\Delta N/\Delta t =$ constant, and may thus compute it for any Δt. For a white-dwarf mass we adopt $0.6 \mathfrak{M}_\odot$. This is based on Greenstein's (1958) statistical determination of $0.56 \mathfrak{M}_\odot$ for white dwarfs and on direct mass determinations which are available for three white dwarfs in visual binaries; these yield 1.0, 0.4, and $0.4 \mathfrak{M}_\odot$. For $\frac{1}{2}T$ of 2×10^8 years we would then expect $0.6 \times 10^3 \mathfrak{M}_\odot$ of interstellar matter in M3. Within the accuracy of the input data we may estimate the mass of interstellar matter in M3 as $\sim 10^3 \mathfrak{M}_\odot$.

TABLE IIIa. The mass, $\mathfrak{M}/\mathfrak{M}_\odot$, of a cloud which would contract under its own gravitational attraction for various values of N_H and T°K, $\mu=1.4$.

N_H/cm^3 \ T°K	10	25	50	100
10	500	2000	5600	16 000
10^2	160	630	1800	5000
5×10^2	70	280	800	2200

Because of the low escape velocity from a globular cluster, ~10 km/sec, evaporation of interstellar gas from the edge of the cluster would occur at relatively low kinetic temperatures ($\gtrsim$50°K). If such evaporation were to go on at a rapid rate, the above values for the interstellar mass in M3 would be far too large. However, if such material were to gather into clouds the evaporation rate would be greatly reduced. It was shown in Sec. II that there is good evidence that such clouds (of dust, at least, and presumably gas) do exist in clusters and we therefore assume that evaporation is not the dominant mechanism for the removal of intraglobular matter.

In summary, we may expect to find $\sim10^3\mathfrak{M}_\odot$ of interstellar matter in M3. This is approximately 0.5% of the present mass of the cluster. Within the range of cluster masses and varying values of the semi-major axes of their orbits, this percentage may be assumed to be representative of globular clusters in general.

IV. EFFECTS ON THE STELLAR POPULATION OF A CLUSTER

Globular clusters have been described as a "dying" population—one in which stars evolve to their final state as white dwarfs or escape completely from the cluster. The presence of interstellar clouds in the cluster may alter this picture. If these clouds are dense and massive enough, stars may form from this interstellar matter and thus add a small number of new stars to the total cluster population.

We may employ the virial theorem to make a rough estimate of the minimum mass of a cloud which will contract under its own gravitational attraction. For contraction we require the second time derivative of the moment of inertia to be negative. This condition will be met if

$$2E<-\Omega,$$

where E is the total kinetic energy of the particles and Ω is the total potential energy. We shall assume that the initial distribution of material is roughly spheri and of radius R, temperature T, and density ρ. V find that for contraction

$$\frac{\mathfrak{M}}{\mathfrak{M}_\odot}\geq1.2\times10^{-10}\left(\frac{T}{\mu}\right)^{\frac{3}{2}}\left(\frac{1}{\rho}\right)^{\frac{1}{2}},$$

where μ is the mean molecular weight. For a hydrog density N_H and $\mu=1.4$, Eq. (6) becomes

$$\mathfrak{M}/\mathfrak{M}_\odot\gtrsim50(T^{\frac{3}{2}}/N_H^{\frac{1}{2}}).$$

Table IIIa contains values of $\mathfrak{M}/\mathfrak{M}_\odot$ for vario combinations of N_H and T.

From previous considerations we expect the mass the cloud to be $\mathfrak{M}\lesssim10^3\mathfrak{M}_\odot$. We see from Table II that we require relatively high densities and l temperatures. The former are not too extrem

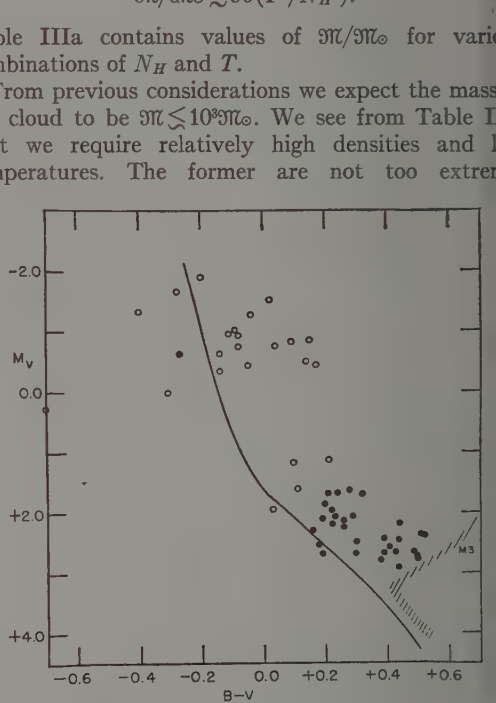

FIG. 5. Composite color-magnitude diagram for the blue st in nine globular clusters. The filled circles represent the stars, the open circles, the stars in the remaining eight clust The age-zero main sequence and the region of the M3 dwarfs subgiants is also shown.

especially in view of the high opacity noted intraglobular clouds. A low temperature may also expected to exist in such opaque clouds.

Table IIIb contains the corresponding radii, parsecs, for a spherical configuration of mass a density corresponding to those of Table IIIa. We ag find that, to be consistent with the apparent sizes the dark nebulae found in globular clusters, we requ densities of several hundreds and temperatures several tens of degrees. A cloud possessing a cent condensation rather than the above assumed unifo density would have a larger gravitational self-ener The requirements on the temperature and dens would then be less extreme (Kahn 1960).

The foregoing considerations apply to the entire clo We may then expect stars to form within this cloud a manner similar to that operating within clo

TABLE IIIb. Radii in parsecs of a spherical cloud of the above mass and density, $\mu=1.4$.

N_H/cm^3 \ T°K	10	25	50	100
10	7.1	11.3	15.9	22.5
10^2	2.3	3.5	5.0	7.1
5×10^2	0.5	1.6	2.2	3.1

isting in the general field. In essence, we would pect a cluster to form within the boundary of a bular cluster. If such a star-formation process had curred relatively recently we would expect to find

(1) Main-sequence stars which are young compared the age of the cluster, i.e., stars which sit above the ister main-sequence turnoff point.
(2) A clustering of such stars within the projected ea of the globular cluster.

ere is evidence that both of these occur in globular isters.

The occurrence of stars above the main-sequence rnoff point in the color-magnitude diagram of globular isters has been noted by Sandage (1953) and by Arp 955). These stars, which are distinct from the rizontal branch stars, are too common to be tributed to field stars superposed on the cluster. An cellent example of such stars is to be found in the lor-magnitude diagram of M3 (Sandage 1953, hnson and Sandage 1956). For convenience in the llowing discussion these stars will be referred to as ue stars. A composite color-magnitude diagram for e blue stars in nine globular clusters is shown in g. 5. The filled circles represent M3 blue stars while e open circles represent the blue stars in the remain- g eight globular clusters. The source material for is figure is given in Table IV. All observations not eady on the B, V system were transformed to this stem except those for M53 which are on the P, V stem and close enough to the B, V system (Cuffey 58) for the present purpose. The M53 star plotted $B-V$ (really $P-V$) $=-0.7$ is an exception to the sumed similarity of the two systems. The age-zero ain sequence and the M3 main-sequence and sub- ant regions are also shown in this figure. The ap- rent separation into two groups of blue stars implied

TABLE IV. References for data used in Fig. 5.

uster	No. blue stars	Apparent modulus	$B-V$ reddening	Reference
M3	31	15.67	0.00	Sandage, A. R. 1953, *Astron. J.* **58**, 61.
M10	4	14.82	0.35	Arp, H. C. 1955, *Astron. J.* **60**, 317.
M2	2	16.15	0.04	Arp, H. C. 1955. *Astron. J.* **60**, 317.
M22	1	14.00	0.44	Arp, H. C. and Melbourne, W. G. 1959, *Astron. J.* **64**, 28.
NGC 4147	3	16.85	0.10	Sandage, A. R. and Walker, M. 1955, *Astron. J.* **60**, 230.
M5	2	15.08	0.14	Arp, H. C. 1955, *Astron. J.* **60**, 317.
M15	1	15.89	0.00	Arp, H. C. 1955, *Astron. J.* **60**, 317
M13	3	14.67	0.14	Arp, H. C. 1955, *Astron. J.* **60**, 317.
M53	7	16.90	0.00	Cuffey, J. 1958, *Astrophys. J.* **128**, 219.

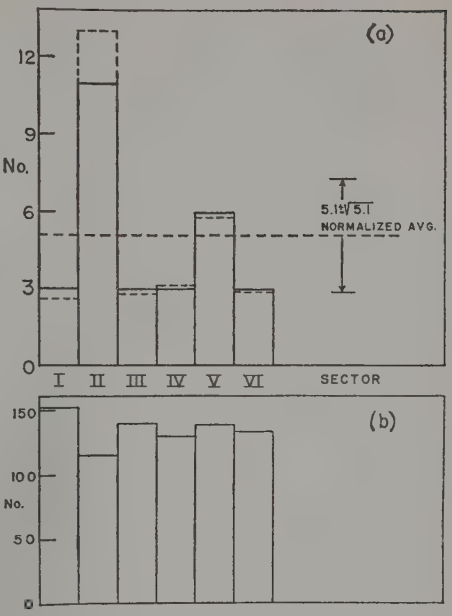

FIG. 6. (a) Solid histogram: the observed angular distribution of the blue stars in M3. Dashed histogram: the blue star distribution corrected for different sized samples of stars available for each sector. (b) Angular distribution of all stars with $m_{pv} \leq 19.00$ in Sandage's catalogue for M3. These data were used to obtain the dashed histogram in (a).

by the color-magnitude diagram is very likely due to a selection effect; many of the clusters were studied only to intrinsically bright magnitudes.

It has been suggested (Sandage 1953) that such blue stars represent some small fraction of the total cluster population which, in their evolutionary processes, have remained well mixed and are therefore evolving essentially up the main sequence rather than to the right into the giant area. Such mixing would, presumably, be due to a very high rotational velocity of the star thus establishing the necessary meridianal circulation currents. However, such high rotational velocities are very rare for the type of star considered here and we must consider this suggestion with some reservation.

A number of globular clusters were examined for the possibility of a clustering tendency among the blue stars. The results for M3 are shown in Fig. 6. This cluster has a good sample of such blue stars which are distinctly separated from the scatter of the main-sequence and subgiant parts of the color-magnitude diagram as well as from the blue horizontal branch stars. There are 29 such blue stars that (i) lie in a region above the turnoff point defined by the following limits: $m_{pv} \leq 19.00$, C.I. < 0.38 and to the left of a line located by the coordinates $m_{pv} = 18.20$, C.I. $= 0.50$ and $m_{pv} = 19.00$, C.I. $= 0.26$, and (ii) are listed in Sandage's (1953) catalogue under Series I and II (Series III does not cover the entire cluster and therefore could not be used).

The distribution of these 29 blue stars within six equally spaced sectors is shown by the solid histogram in Fig. 6(a). Eleven of these blue stars lie in one sector. The number of all stars brighter than $m_{pv}=19.00$ in Sandage's catalogue is not evenly distributed among the six sectors. Except for crowding and variables, the stars included in the catalogue were randomly chosen (Sandage 1959) and do not necessarily indicate the actual angular distribution of the cluster stars. An incompleteness factor must thus be applied to the numbers of blue stars per sector to adjust for this uneven catalogue coverage. When normalized to the average number of all stars per sector, the number of blue stars becomes 30.5; thus, one would expect $5.1\pm(5.1)^{\frac{1}{2}}$ blue stars per sector. Instead, almost one-half of this normalized number of blue stars (13) are found in just one sector. The formal probability of finding 13 or more stars in a sector is less than 0.014. The normalized distribution of the blue stars is shown by the dashed histogram in Fig. 6(a). The distribution of all catalogue stars brighter than $m_{pv}=19.00$ is shown in Fig. 6(b).

Unfortunately, the other globular clusters for which C-M diagrams and catalogues are available show too few blue stars for any significant conclusion to be drawn. One possible exception is M10. This cluster has been studied by Arp (1955) to a magnitude limit only a bit fainter than the horizontal branch. He found four rather bright blue stars. These are numbers I-32, I-33, I-34 and III-48, and may be identified in Arp's Fig. 3. Three of these stars fall within a circle of 18″ radius; this is an area only 0.25% of the total area studied by Arp. If they are at the same distance within the cluster, they are separated by less than one parsec. These numbers must be viewed with great caution. Not only are the stars few, but other clusters which contain a similar small number of known blue stars do not show this clustering effect. Further, these bright blue stars may have an origin different from the fainter blue stars found nearer the main-sequence turnoff point.

If these blue stars are indeed newly formed within the globular cluster we would expect that they would initially move as a group through the cluster. It is likely that such motion would carry the group close to the central regions of the cluster. The effect of this would be twofold: (1) the shorter relaxation time in this region would cause the group of stars to disperse and (2) any remnants of the cloud from which the stars were formed would also be dispersed. This latter mechanism can be expected to be operative for any intraglobular cloud in general. Since several oscillations through the cluster would be necessary for significant tidal disruption, the time scale would be similar to that for the period of oscillation through the galactic plane and so need not affect the previous arguments.

The formation of the blue stars has to satisfy another requirement—that of the time necessary for the stars to contract from some low-density condensation with the cloud. We may set as an upper limit for this ti the period of oscillation through a globular cluster a star (or cloud) situated near the edge of the clust This is about 3×10^7 years. The contraction time f the latest type star that might be considered here, F is $\sim1.3\times10^7$ years. Thus, a blue star may form in time short compared to the period of oscillation of cloud through the cluster. The presence and appare clustering of the blue stars are thus an expect by-product of the interstellar matter in globular cluste

Another mechanism for creating and clustering t blue stars is accretion. The possibility that accreti could explain the occurrence of early type stars in t general field has generally been abandoned. T problem of the relative motion of stars and clou proved too formidable. In a globular cluster, th problem does not exist. The velocity dispersion mu be relatively small, otherwise the star or cloud wou escape. It is thus important to examine accreti quantitatively to determine if it is a competing mech nism with star formation.

The accretion rate (Bondi and Hoyle 1944) is giv by

$$d\mathfrak{M}/dt=\alpha(2\pi\rho G^2\mathfrak{M}^2/u^3), \qquad (7$$

where $\mathfrak{M}$ = mass of star
ρ = density of cloud
u = relative velocity of star and cloud
G = gravitational constant,

and α is a numerical factor which depends upon t way in which the accretion stream has been establishe It has a value between 1 and 2.

The cloud will retard the motion of the star; f $u=0$, Bondi (1952) obtains in place of Eq. (8)

$$d\mathfrak{M}/dt=\alpha'(2\pi\rho G^2\mathfrak{M}^2/C^3), \qquad (7$$

where C is the velocity of sound at infinity a $0.5\leq\alpha'\leq2.24$.

The time, t_1, and distance x_1, for u_0, the initi velocity, to be reduced to a value somewhat less tha C have been derived by McCrea (1933). He obtains

$$t_1=\frac{u_0^3}{(4\alpha+3\beta)2\pi\rho G^2\mathfrak{M}_0} \qquad (1$$

$$x_1=\frac{u_0^4}{(5\alpha+4\beta)2\pi\rho G^2\mathfrak{M}_0}; \qquad (1$$

here, $\mathfrak{M}_0$ is the initial mass of the accreting sta Following McCrea we shall adopt $\alpha=2$ and $\beta=10$.

For a star trapped in the cloud ($u<C$) integrati of Eq. (9) gives the time for the star to increase i mass by an amount $\Delta\mathfrak{M}$ to some new value $\mathfrak{M}$, thus

$$t_2-t_1=\frac{C^3}{\alpha'2\pi\rho G^2}\left[\frac{1}{\mathfrak{M}_0}-\frac{1}{\mathfrak{M}}\right]. \qquad (1$$

is then the total time for the process, i.e., to stop the
ır and to add mass $\Delta\mathfrak{M}$.
The conditions of the problem require that

(i) x_1 be small compared to the cluster diameter,
(ii) t_2 be less than the time between passages through
e galactic plane,
(iii) t_2 be less than the time for the blue stars to
olve off the main sequence.

r (i) we may take x_1 to be of the order of one-tenth
a cluster diameter, or about five parsecs. Values of
$t_2 \sim 10^8$ years will satisfy (ii) and in most cases (iii).
Tables Va and Vb give values of x_1 and t_2 for various
drogen densities, N_H, and percentage mass increase.
) evaluate Eqs. (10)–(12) the following were adopted:
$= 1$ km/sec, $\alpha' = 2.24$ (isothermal case), $\mathfrak{M}_0 = 1\mathfrak{M}_\odot$, μ
ıe mean molecular weight) $= 1.4$, and $C = 0.55$ km/sec.
The sequence of events which would have to occur
ould involve the capture of a number of stars of
out solar mass by a very dense and relatively large
oud. Initially, these stars would have just a small
locity difference from that of the cloud—enough to
ing them into the cloud. Once in the cloud these
ars would accrete varying and relatively small
ıounts of mass and as a result increase their lumi-
sity and temperature, thus moving them into another
rt of the color-magnitude diagram. Eventually the
oud would be destroyed or removed from the cluster
s in the case of the formation of the stars) leaving a
all group of stars whose kinematic and physical
operties have been altered. As this group moves
rough the cluster, interactions with the general field
cluster stars will cause the group to disperse (again
in the formation case). Thus both the occurrence
d clustering of the blue stars can be accounted for.
The data of Tables Va and Vb indicate that, within
e approximations of the input data, accretion can
ke place. However, the requirements here (N_H and x_1)
e more extreme than those for the case of regular
ar formation and we would expect that if we had such
uds they would just as likely condense into stars.
e may therefore conclude that accretion, though
ssible, is not the principal mechanism for the forma-
n of the blue stars.
Throughout this discussion we have assumed that
e admittedly scanty data on the clustering of the
ue stars represent a real clustering and not just a
ance occurrence. From the data presently available

TABLE Va. The time t_2 (in years) for various values of N_H and the final mass of the star, $\mathfrak{M}/\mathfrak{M}_\odot$.

N_H/cm³ \ $\mathfrak{M}/\mathfrak{M}_\odot$	1.1	1.5	2.0	5.0	10.0
10	7.8	10.3	15.2	20.2	22.2×10^8
10^2	7.8	10.3	15.2	20.2	22.2×10^7
5×10^2	1.5	2.0	3.0	4.1	4.4×10^7
10^3	7.8	10.3	15.2	20.2	22.2×10^6

TABLE Vb. The distance x_1 and the corresponding mass of a spherical cloud of this diameter.

N_H/cm³	$x_1$pc	$\mathfrak{M}/\mathfrak{M}_\odot$
10	4.8×10^2	1.9×10^7
10^2	4.8×10	1.9×10^5
5×10^2	9.6	7.8×10^3
10^3	4.8	1.9×10^3

such an assumption seems reasonable. An obvious desideratum is more information on the numbers and distribution of blue stars in clusters; this will primarily come from color-magnitude diagrams which extend to relatively faint magnitudes. We need not expect that all globular clusters will contain blue stars. It also follows that if the reality of the clustering of the blue stars is firmly established, the possible explanations of the existence of these blue stars in globular clusters seems pretty well restricted to the two given here. It should also be kept in mind that there may be at least two distinct classes of blue stars, one possibly being represented by the subluminous O-type star in M3 and the other by the large number of fainter blue stars which are also found in M3.

V. SUMMARY

Various methods of detecting interstellar matter in globular clusters have been discussed. It was shown that H II regions and their characteristic emission lines are very unlikely in a globular cluster. Further, the interpretation of even weak 21-cm emission is difficult because of a lack of knowledge of the physical conditions of intraglobular matter, especially the ratio of atomic to molecular hydrogen. The only method available at present is that of the obscuring effect of interstellar dust.

There is evidence that such dust (and presumably gas) clouds are present in globular clusters. This is shown by the large number of obscured regions found in globular clusters. It is difficult to attribute all of these obscured regions to relatively close foreground clouds; the number required by such an explanation is too large. In addition, such close and opaque clouds would need to have large fluctuations in opacity to account for the appearance on long-exposure photographs of stars superposed on the obscured regions. The likelihood that these regions are due to a statistical fluctuation in the stellar distribution was shown to be small.

This intraglobular material can be attributed to the shedding of mass by stars evolving to the white-dwarf stage. A significant amount of such material will collect in a globular cluster between passages of the cluster through the galactic plane. The collection of such matter into dense clouds could result in the formation of new stars. This would account for those stars which sit above the main-sequence turnoff point in the color-magnitude diagrams of some globular clusters. Such

an explanation would further predict that these stars would have a nonrandom distribution in the cluster. The scanty data thus far available indicate that this is indeed the case.

REFERENCES

Arp, H. C. 1955, *Astron. J.* **60**, 317.
Bok, B. J. 1948, *Harvard Obs. Monograph No. 7, Centennial Symposia*, p. 53.
Bok, B. J. and Reilly, E. F. 1947, *Astrophys. J.* **105**, 255.
Bondi, H. 1952, *Monthly Notices Roy. Astron. Soc.* **104**, 273.
Clerke, A. M. 1903, *Problems in Astrophysics* (A & C Black, London, England), Chap. 30.
Cuffey, J. 1958, *Astrophys. J.* **128**, 219.
FitzGerald, A. P. 1955, *Irish Astron. J.* **3**, 204.
Greenstein, J. L. 1958, *Handbuch der Physik*, edited by S. Flügge (Springer-Verlag, Berlin, Germany), **50**, 161.
Hoerner, von S. 1955, *Z. Astrophys.* **35**, 255.
Hogg, H. S. 1959a, *Handbuch der Physik*, edited by S. Flügge (Springer-Verlag, Berlin, Germany), **53**, 185.
——. 1959b, *Astron. J.* **64**, 425.
Holden, E. S. 1891, *Publs. Astron. Soc. Pacific* **3**, 375.
Hoyle, F. and Schwarzschild, M. 1955, *Astrophys. J. Suppl.* No. 13.
Idlis, G. M. and Nikolsky, G. M. 1959, *Astron. J. U.S.S.R.* **36**, 6
Johnson, H. L. and Sandage, A. R. 1956, *Astrophys. J.* **124**, 3
Kahn, F. D. 1960, in *Die Entstehung von Sternen*, by G. Burbidge, F. D. Kahn, R. Ebert, S. v. Hoerner and Temesváry (Springer-Verlag, Berlin, Germany), p. 104.
McCrea, W. H. 1953, *Monthly Notices Roy. Astron. Soc.* **113**,
Mayall, N. U. 1946, *Astrophys. J.* **104**, 290.
Minkowski, R. and Osterbrock, D. 1959, *Astrophys. J.* **129**, 5
Mowbray, A. G. 1946, *Astrophys. J.* **104**, 47.
Roberts, M. S. 1956, *Astron. J.* **61**, 195.
——. 1959, *Nature*, **184**, 1555.
Rosse, Earle of. 1861, *Phil. Trans. Roy. Soc. London* **151**, plate
Sandage, A. R. 1953, *Astron. J.* **58**, 61.
——. 1957, *Astrophys. J.* **125**, 422.
——. 1959, private communication.
Shapley, H. 1915, *Contrib. Mt. Wilson Solar Obs.* No. 116.
Stebbins, J. 1950, *Monthly Notices Roy. Astron. Soc.* **110**, 416.
Strömgren, B. 1948, *Astrophys. J.* **108**, 242.
Takebe, H. and Matsunami, N. 1957, *Publs. Astron. Soc. Jap.* **9**, 136.
Triplett, L. H. C. 1952, *Tracts for Computers* (Cambridge University Press, London, England).

THE ASTRONOMICAL JOURNAL VOLUME 65, NUMBER 8 OCTOBER, 19

The Wavelength Dependence of Polarization. I. Instrumental Polarization*

THOMAS GEHRELS
Goethe Link Observatory, Indiana University, Bloomington, Indiana

(Received May 31, 1960)

Measures on nonpolarized stars are reported for the McDonald 82-inch and 36-inch and for the Goethe Link 36-inch reflectors. For different telescopes the amount of instrumental polarization differs greatly. The polarization increases toward the ultraviolet. The instrumental effects may cause photometric as well as polarimetric errors, and a method to avoid them (Thiessen and Broglia 1959) is referred to.

Measures on depolarization effects are reported and small corrections are derived for incomplete action of the depolarizer disks and of the Wollaston prism. Depolarization by the mirrors of the 82-inch telescope is found to be negligible.

INTRODUCTION

THE main purpose of this series of papers is to compare interplanetary and interstellar particles, with measures of polarization and color over a wide range of wavelengths. In order to cover a wide range of wavelengths, and to depend as little as possible on weather conditions, a Wollaston photometer was built that uses a depolarizer for calibrations; the ordinary and extraordinary rays are measured with two multiplier phototubes by simultaneous integrations. The photometer has been described (Gehrels and Teska 1960); the effectiveness of the depolarizer was checked with each of the wide-band filters in use.

Preliminary results have been published for stars, reflection nebulae, Venus, Mars, the moon, and the sunlit blue sky [diagrams and further references were presented (Gehrels 1960a) at a *Polarization Conference* sponsored by the National Science Foundation and by the Lowell Observatory]. The detailed observations will be given in this series. Paper I describes the corrections for spurious polarization, introduced by aluminiz mirrors, and a method to avoid the effects in the futu

Dollfus (1957) observed the polarization by telesco mirrors, of normally incident light; the following co clusions are drawn from his work. (1) Dollfus has r found any instrumental polarization on silvered mirro silvered either chemically or in vacuum. (2) So aluminized mirrors, aluminized in vacuum, show stro effects, while others do not. (3) The polarization var very much over the mirror surface. (4) The effe appear to be caused by the coating rather than by i perfections of the mirror polish.

Thiessen and Broglia (1959) are studying the effe extensively, and preliminary conclusions are dra from their experiments. (5) The instrumental pola zation is not caused by the aluminum evaporati being at an angle different from normal to the surfa For steep angles, however, the conclusion may be d ferent (see later). (6) The instrumental polarization caused by the glow discharge, for final cleaning of t mirror, being at an angle different from normal to t surface. Presumably, the asymmetric potential or gl discharge establishes an electric field in a thin surfa

* Publications of the Goethe Link Observatory, No. 40. This program is supported by the Office of Naval Research.

ver, such that the aluminum is aligned in a crystalline ructure. (7) The amount of polarization is independent the thickness of the coating; the orientation of polar- tion is with the electric vector maximum parallel the electrode. Presumably, the crystals are aligned rpendicular to the electrode and the polarization is differential absorption. (8) Not all mirrors with lique glow-discharge show instrumental polarization, d the observed amounts vary widely. The polarization parently occurs only if the crystalline dimensions ve reached a critical value with respect to the wave- gth of light.

When the angle of evaporation differs greatly from rmal to the surface, by more than 70°, the above con- sions (1) and (5) may no longer be correct. Reimer 957) deposited metals very obliquely, in layers with ckness of about 0.04 micron, and he found strong larizations in the *transmitted* light.

For polarization measures of greater precision than at of the present program, effects of image formation the cathode and of instrumental circular polarization ve to be taken into account. These effects have been scussed by Behr (1960) and by Serkowski (1960), pectively.

THE OBSERVATIONS

The instrumental polarization is observed on stars at are chosen because of parallax greater than 0".02 d/or because no polarization was found by other servers. At least five stars per observing period are served for this purpose. A table of corrections is tained from the observations, after change of sign, the individual photometer orientations (180, 270, 0, 240, 120, and 210 deg), an example of which is own in Table II of the description of the photometer ehrels and Teska 1960). In order to avoid the sys- matic effect of instrumental polarization, all our servations are corrected with such tables.

After least-squares solution of the values in the cor- tion tables, but with signs of the original observa- ns, the instrumental polarizations are listed in ble I. Wavelengths are given in terms of $1/\lambda$, the erse of the effective wavelength in microns. The me "effective wavelength" is used here for

$$\lambda = \int S(\lambda)\lambda d\lambda / \int S(\lambda) d\lambda,$$

ere $S(\lambda)$ is the response of the tubes to the part of ite light transmitted by the filter, according to nufacturers' specifications. The percentage polari- ion is $P = 100(I_1 - I_2)/(I_1 + I_2)$, where I_1 and I_2 are intensity of electric vector maximum and minimum, pectively; and θ is the equatorial position angle of electric vector maximum. The results of the Donald 36-inch in Table I agree closely with the rections for instrumental polarization published by hr (1960). The measures at the Goethe Link Ob- vatory were made by R. E. Samuelson as a part of rogram on Venus.

TABLE I. Observations of instrumental polarization.

Tel.[a]	$1/\lambda$	Period [b]	P	θ	$\bar{P}$
			%		
82″	1.01	Apr. 17–22	0.06	5°.4	%
		Apr. 23–30	0.12	135.3	
		July/Aug.	0.20	67.9	0.18
		Apr. 1960	0.32	146.2	
82″	1.46	July/Aug.	0.13	81.0	0.13
82″	1.79	Oct. 1958	0.05	...	
		Apr. 17–22	0.19	26.5	
		Apr. 23–30	0.06	171.5	0.09
		July/Aug.	0.07	168.5	
		Apr. 1960	0.08	5.7	
82″	2.38	July/Aug.	0.12	164.4	0.12
82″	2.79	Apr. 17–22	0.48	179.3	
		Apr. 23–30	0.44	171.5	0.48
		July/Aug.	0.45	168.9	
		Apr. 1960	0.56	178.2	
82″	3.08	July/Aug.	0.63	167.9	0.63
36″	1.01	May	0.12:	175.2:	0.16
		December	0.17	141.2	
36″	1.46	December	0.12	37.7	0.12
36″	1.79	Dec. 1958	0.35:	...	
		February	0.36	...	0.38
		May	0.64:	12.8:	
		December	0.27	18.1	
36″	2.38	December	0.98	26.2	0.98
36″	2.79	May	2.22:	18.2:	1.96
		December	1.87	20.8	
36″	3.08	December	1.97	23.7	1.97
GL	1.01	Oct./Nov.	0.08	99.2	
		Dec. 1–16	0.34	106.0	0.18
		Feb. 1960	0.12	147.3	
GL	1.46	Oct./Nov.	0.07	124.0	
		Dec. 1–16	0.05	99.1	0.09
		Feb. 1960	0.15	118.1	
GL	1.79	Oct./Nov.	0.16	109.3	
		Dec. 1–16	0.22	110.9	0.14
		Feb. 1960	0.04	141.1	
GL	2.38	Oct./Nov.	0.12	90.4	
		Dec. 1–16	0.10	96.4	0.13
		Feb. 1960	0.17	120.7	
GL	2.79	Oct./Nov.	0.14	106.3	
		Dec. 1–16	0.15	89.5	0.11
		Feb. 1960	0.05	90.6	
GL	3.08	Oct./Nov.	0.19	102.1	
		Dec. 1–16	0.16	76.6	0.19
		Feb. 1960	0.21	105.6	

[a] 82″ = McDonald 82-inch, at Cassegrain; 36″ = McDonald 36-inch, at Cassegrain; and GL = Goethe Link 36-inch, at prime focus.
[b] Observing periods in 1959, unless stated otherwise.

The precision of the mean values in the correction tables is found from the repetition of the individual determinations, namely ±0.0014 mag. (p.e.) ±0.0004; after least-squares solution of the values at 6 orientations the probable error in Table I is ±0.0007 mag., or ±0.03%±0.01. This is to be compared with the probable error found from the results on strongly polarized stars, in Paper II (Gehrels 1960b), namely ±0.07%. The precision of the results in this program is little affected by instrumental polarization, especially when, in future work, nonpolarized stars are observed more often.

The scatter of the individual results about their average, for each telescope and filter in Table I, gives a probable error of 0.04%±0.01. The agreement of the above numbers ±0.03% and ±0.04% indicates that the instrumental polarizations depend little, if at all,

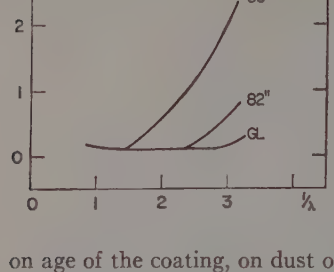

FIG. 1. Percentage polarization, introduced by aluminized mirrors, versus the inverse of the effective wavelength in microns. For the McDonald 36-inch and 82-inch and for the Goethe Link telescope.

on age of the coating, on dust on the mirror, or on the alignment of mirror and photometer axes. The Goethe Link mirror had been re-aluminized immediately before the observing period of Oct./Nov., 1959. The 82-inch mirror had been washed prior to the run of April, 1960. For each observing session, the axis of the photometer is aligned again with that of the mirror(s). However, these conclusions are based mostly on the data for the 82-inch and Goethe Link telescopes, whereas the large effects of the McDonald 36-inch may be more uncertain and different for stars of different colors (Behr 1960).

WAVELENGTH DEPENDENCE

Table I shows large differences between different telescopes, but the three reflectors have the low values at longer wavelengths in common. The large scatter of the position angles suggests that some of the small polarizations at longer wavelengths may not be real. The wavelength dependence for each telescope is shown in Fig. 1, with a line drawn through the averages of the last column in Table I.

If the instrumental polarization is due to differential absorption by crystalline elements, such absorption would occur twice, namely upon incidence of the light and again after reflection by underlying parts of the coating (thickness usually about 0.1 micron). The crystal diameter, $2a$, may perhaps be estimated with calculations of the extinction by aligned metallic cylinders (van de Hulst 1957). The strongest polarization in van de Hulst's Fig. 69 occurs at $2\pi a/\lambda \simeq 0.3$, so that for the mirror(s) of the McDonald 36-inch $2a \simeq 0.02$ microns, and possibly smaller for those of the 82-inch. With observations at wavelengths shorter than 3000 A, one might obtain the shape of Fig. 6 of Paper II (Gehrels 1960b). This explanation, however, is very tentative; multiple-reflection phenomena might explain the observed polarizations. Electron-microscopic studies of the mirror surfaces, as in Reimer's work, with a determination of dimensions and alignment of the crystalline structure, would be decisive.

THE AVOIDANCE OF INSTRUMENTAL POLARIZATION

Instrumental polarization may cause small systematic errors in photometry as well as in polarimetry. The photometric errors, caused by the spurious polarization, in stellar work with the McDonald 36-inch are less than 0.001 mag. But if a telescope with 5% instrumental polarization were to be used on an object with 20% polarization, a reflection nebula for instance, systematic error up to 0.01 mag. could appear. Incidentally, a Newtonian telescope may have about 5% instrumental polarization. It is especially important for high precision in polarimetry to avoid the instrumental effects.

Telescope mirrors usually are aluminized with an evaporation normal, at least symmetrical, to the mirror surface. In addition, the glow discharge should be normal to the surface. Even so, a small residual polarization may be found, the cause of which is being studied at the Hamburg Observatory (Thiessen, personal communication). Thiessen and Broglia are using electrode disks that are, parallel to the surface, slightly larger than the mirror; only in one case until now was there a small amount of instrumental polarization left. The Goethe Link mirror was aluminized with complete symmetry, by Leroy M. E. Clausing of Skokie, Illinois, and the results are good, as shown before. Mr. Clausing uses the glow discharge sparingly as he has observed (personal communication) that it causes a thin surface layer, presumably consisting of oxidized oil. This observed surface layer may actually be the one postulated by Thiessen and Broglia.

TESTS OF DEPOLARIZATION

The effectiveness of the depolarizer is occasionally checked by rotating a piece of Polaroid HN 32 (Polaroid HR for the infrared) in front of the photometer while the depolarizer is in the beam. The rotation causes a change of 1.2 units, of the nearly 100 units amplifier deflection for one of the tubes; this means a spurious depolarization of 1.2 in what is supposedly 100% polarization. The effect is probably due to nonperfect orientation of the optical axes of the two depolarizing disks. The checks are made with our combinations of tubes and filters for $1/\lambda = 1.01$, 1.46, 1.79, and 2.[illegible]. No wavelength dependence has been observed. At $1/\lambda = 2.38$ and 3.08, the checks can be only qualitative using the strong polarization of the sunlit blue sky as a source, because the Polaroid is not effective at these wavelengths. The depolarizer breaks down when a much narrower filter is used, such as half-standard thickness of Corning 2030 combined with a 1P21 tube.

The effectiveness of the depolarizer and the Wollaston prism combined was checked with another Wollaston in front of the photometer. The percentage polarization of the ordinary and extraordinary rays was determined with the IBM 650 as usual, and the results are listed in the first part of Table II. Allowing for the fact that two Wollaston prisms are involved, a depolarization effect is found of 2.5 per 97.5% observed polarization (3.6 per 96.4% observed polarization in the ultraviolet), which in each case 1.2% is due to the disks of the depolarizer. The amounts for the present photometer m

TABLE II. Observed polarization of injected light.

Source	Location	1/λ	P
			%
Wollaston prism, ordinary ray	Directly into photometer	1.01	94.9
		1.79	96.5
		2.79	94.2
Wollaston prism, extraordinary ray	Directly into photometer	1.01	96.8
		1.79	96.0
		2.79	94.0
Transmitted by stack of nine glass plates	290°–35″	1.01	77.9
		1.79	81.0
		2.79	86.3
	295°–23″	1.01	77.9
		1.79	80.7
		2.79	86.8
	Directly into photometer	1.01	77.2
		1.79	77.5
		2.79	82.1
	58°–17″	1.01	77.6
		1.79	80.9
		2.79	85.1
	70°–28″	1.01	77.6
		1.79	77.4
		2.79	85.4
	Directly into photometer	1.01	73.9
		1.79	77.0
		2.79	86.0

ctually be slightly smaller as the second Wollaston, hat was used for the beam, has two cracks. The depolarization effect is probably caused by multiple cattering inside the Wollaston prism; the wavelength lependence of the effect seems to confirm this explanation.

Depolarization by the two aluminized mirrors of the 2-inch telescope was looked for with a 1-inch beam ransmitted by a stack of nine thin crown-glass plates, he angle of incidence being the Brewster angle (for ach color). In otherwise perfect darkness the beam was ent, parallel to the telescope axis, either incident on a mall portion of the primary mirror or directly into the hotometer. The measures were made in August 1960; they are listed in the second part of Table II. The location of incidence on the 82-inch mirror is given for the telescope east of the pier and pointed toward the zenith. For instance, 290°–35″ means a spot at azimuth (counted from the north through the east) 290° and at a distance of 35 inches from the center of the mirror. The measures were actually made with the telescope in a more horizontal, more accessible, position. After reflection by the mirrors the polarizations are not less than when the beam goes directly into the photometer; the mirrors do not show any depolarization. The larger scatter of the observations that have the light directly into the photometer is due to the more difficult alignment in that position. Incidentally, the observed amounts of polarization are appreciably larger than the predicted ones (see Jenkins and White 1957), 61.6% at $1/\lambda = 1.01$, 62.7% at $1/\lambda = 1.79$, and 64.7 at $1/\lambda = 2.79$.

The conclusions on depolarization are summarized with the following example: When the observed amount of polarization is 10.00%, the correction for depolarization should be +0.26 (+0.37 in the ultraviolet), of which 0.12 is due to the depolarizer and the remainder to scattered light within the Wollaston prism. Aluminized telescope mirrors, probably in general, do not cause an appreciable amount of depolarization.

REFERENCES

Behr, A. 1960, *Lowell Obs. Bull.* **4**, 292.
Dollfus, A. 1957, *Ann. d'Astrophys. Suppl.* **4**, 32.
Gehrels, T. 1960a, *Lowell Obs. Bull.* **4**, 300.
——. 1960*b*, *Astron. J.* **65**, 470 (Paper II).
Gehrels, T. and Teska, T. M. 1960, *Publs. Astron. Soc. Pacific* **72**, 115.
Hulst, H. C. van de. 1957, *Light Scattering by Small Particles* (John Wiley & Sons, Inc., New York).
Jenkins, F. A. and White, H. E. 1957, *Fundamentals of Optics* (McGraw-Hill Book Company, Inc., New York), Chap. 24.
Reimer, L. 1957, *Optik* **14**, 82.
Serkowski, K. 1960, *Lowell Obs. Bull.* **4**, 296.
Thiessen, G. and Broglia, P. 1959, *Z. Astrophys.* **48**, 81.

The Wavelength Dependence of Polarization. II. Interstellar Polarization*

THOMAS GEHRELS
Goethe Link Observatory, Indiana University, Bloomington, Indiana
(Received May 31, 1960)

The probable error of the polarization measures is ±0.07%, or ±0.0015 mag., found from observations made under various weather conditions. The interstellar polarization has a maximum at 6500 A, decreasing sharply toward longer and gradually toward shorter wavelengths. The wavelength dependence is qualitatively interpreted with computations (van de Hulst 1957) of the extinction by aligned cylinders. Particle sizes of 0.05–0.49 microns are derived for various refractive indices; the agreement of observations and calculations is equally good for metallic and dielectric particles.

IN the first part of this paper the performance of the photometer is checked by comparing observations on strongly polarized stars with results obtained by other observers. The second part deals with a remarkable wavelength dependence found for the interstellar polarization. This wavelength dependence had been qualitatively predicted by Davis and Greenstein in 1951 and was discussed more recently by Davis (1959). The infrared part has been observed by Hiltner (Strömgren 1956), while some decrease in the ultraviolet has been found by Behr (1959).

THE OBSERVATIONS

Eight stars were observed for the purpose of a comparison with existing data. The observations are listed in Table I; they were made with the McDonald 82-inch, except for the ones of May 2, 1959, which were made with the McDonald 36-inch reflector. The stars are arranged in order of galactic longitude, the symbols have been explained in Paper I (Gehrels 1960), and $p=P/46.05$. Colons are used when the average of the residuals in the least-squares solution is greater than 0.30%.

The precision is found from internal agreement of the repeated observations, giving half-weight to the values with a colon. The amount of polarization has a probable error of ±0.07%, or 0.0015 mag.; the probable error of the position angles is ±2°.7. Some of the measures were made through clouds and with poor seeing; the results were not affected. The precision for a faint object is, of course, better when more light gets through. The over-all precision may therefore be slightly improved by observing under excellent conditions only.

It is seen in the fifth column of Table I that some nights give position angles systematically different from those of other nights. The differences, although always less than 5°, seem to indicate a systematic error of unknown cause.

The last three columns of Table I give the comparison with results of other observers, taken from a summary of references, effective wavelengths, and data, by Serkowski (1960). The agreement with the other observers is well within the observational precisions. Corrections for depolarization, as derived in Paper I, ha not yet been applied to the present results.

WAVELENGTH DEPENDENCE

The polarizations of Table I are repeated in Table after normalization to the average amounts of H 183143 at $1/\lambda=1.46$ and 1.79. Also listed are the galac longitude and latitude with respect to the Lund po Until more stars have been observed, one may conclu that the values in the infrared are nearly the same. T values in the ultraviolet may differ, but this, if re is a very slight effect. Another, but incomplete a therefore omitted, observation of HD 42379 casts dou on the high value of P for $1/\lambda=2.79$. There is obvio need for more observations, of stars at different distanc as well as at different longitudes, and with caref determinations of depolarization corrections and of t effective wavelength for each star and filter.

The averages of the eight stars are in the botto line of Table II; values with a colon were given ha weight. The averages are plotted in Fig. 1; the cir radius indicates the probable error of each point, determined from the agreement of the eight stars. flat maximum of polarization occurs near $\lambda=6500$ The line through $1/\lambda=1.01$ may actually be steep with the turnover at longer wavelength than that Fig. 1; narrow-band observations between $1/\lambda=1.$ and 1.46 would be useful.

INTERPRETATION

The interpretation of Fig. 1 is based on calculatio of the extinction by long cylinders (perpendicular

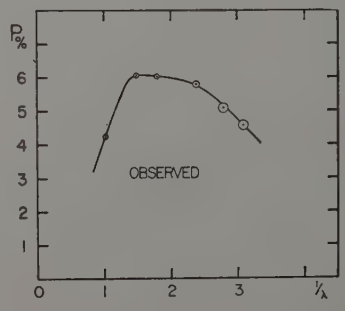

FIG. 1. Observed p centage polarization, erage of eight stars, a function of the inve of the wavelength microns.

* Publications of the Goethe Link Observatory, No. 41. This program is supported by the Office of Naval Research.

TABLE I. Observations, averages, and comparison with other observers.

Date UT 1959	1/λ	Repeated obs. P	Repeated obs. θ	Single obs. and averages P	Single obs. and averages p	Single obs. and averages θ	Compared with p	Compared with θ	Compared with Observer
		%		%					
Apr. 28	1.01	2.99	71°2	2.89	0m063	68°			
July 31	1.01	2.78	64.8						
July 30	1.46	...	...	4.24	0.092	65			
Apr. 28	1.79	4.11	68.4	4.08	0.089	66	0m110	62°	Hall
July 31	1.79	4.05	62.8				0.077	66	v. P. Smith
July 30	2.38	...	...	3.98	0.086	62			
Apr. 28	2.79	3.01	70.1	3.00	0.065	68			
July 31	2.79	2.98	65.8						
July 30	3.08	...	...	3.07	0.067	63			
Apr. 28	1.01	2.72	88.7						
July 31	1.01	2.51	85·9	2.62	0.057	89			
Aug. 6	1.01	2.64	92.5						
July 30	1.46	...	...	3.75	0.081	86			
Apr. 28	1.79	3.71	91.0				0.072	88	Hall
July 31	1.79	3.65	85.8	3.68	0.080	89	0.077	88	v. P. Smith
Aug. 6	1.79	3.68	90·8						
July 30	2.38	...	...	3.42	0.074	86			
Apr. 28	2.79	2.87	91.4						
July 31	2.79	2.80	86.1	2.87	0.062	89			
Aug. 6	2.79	2.94	89.1						
July 30	3.08	...	...	2.60	0.056	87			
Apr. 30	1.01	...	...	4.21	0.091	0			
Aug. 1	1.46	6.03	177.0	5.99	0.130	179			
Aug. 5	1.46	5.94	1.4				0.126	178	Behr
Apr. 30	1.79	...	...	6.08	0.132	1	0.143	179	Hall
Aug. 1	2.38	5.68	178.7	5.68	0.123	1	0.130	179	Hiltner
Aug. 5	2.38	5.67	3.1				0.147	0	v. P. Smith
Apr. 30	2.79	...	...	5.18:	0.112:	0:			
Aug. 1	3.08	3.94:	178.3:	4.28:	0.093:	0:			
Aug. 5	3.08	4.61:	2.2:						
May 2	1.01	1.85	1.8	1.93	0.042	178			
July 31	1.01	2.01	175.1						
Aug. 1	1.46	2.64	179.5	2.79	0.061	1			
Aug. 5	1.46	2.93	2.1						
May 2	1.79	2.72	179.0	2.73	0.059	178	0.062	2	Behr
July 31	1.79	2.73	177.1				0.068	4	Hall
Aug. 1	2.38	2.76	179.1	2.72	0.059	0	0.061	5	Hiltner
Aug. 5	2.38	2.67	1.6						
May 2	2.79	2.31	5.3	2.36	0.051	2			
July 31	2.79	2.40	178.0						
Aug. 1	3.08	2.33	177.5	2.26	0.049	3			
Aug. 5	3.08	2.19	8.2						
Aug. 8	1.01	...	...	2.11	0.046	119			
Aug. 2	1.46	...	...	3.26	0.071	114	0.074	115	Behr
Aug. 8	1.79	...	...	3.27	0.071	115	0.072	115	Hall
Aug. 2	2.38	...	...	3.25	0.071	113	0.075	117	Hiltner
Aug. 8	2.79	...	...	2.92	0.063	117	0.074	119	Serkowski
Aug. 2	3.08	...	...	2.74:	0.060	117:			
Apr. 28	1.01	...	...	1.92	0.042	169	0.066	172	Behr
Apr. 28	1.79	...	...	2.51	0.055	172	0.058	169	Hall
Apr. 28	2.79	...	...	2.23	0.048	172	0.062	170	Hiltner
							0.068	172	Serkowski
Apr. 29	1.01	...	...	1.85	0.040	168			
Apr. 29	1.79	...	...	2.63	0.057	174	0.074	176	Hall
Apr. 29	2.79	...	...	2.90:	0.063:	168:	0.060	170	Hiltner
Apr. 29	1.01	...	...	2.00	0.043	179			
Apr. 29	1.79	...	...	2.83	0.061	176	0.048	176	Behr
Apr. 29	2.79	...	...	2.23	0.048	178	0.065	177	Hall

ence), made by van de Hulst and by Mrs. van P. ith (van de Hulst 1957). In Figs. 2–6 the observed arization is given with the drawn curve, copied from . 1 without change. The open circles give computed nts as obtained from van de Hulst's Figs. 69 and 71, circle radius indicates the precision of transfer from original figures. The difference (Q_1-Q_2) is taken, ere Q_1 and Q_2 are the efficiency factors for extinction when the electric vector is, respectively, parallel and perpendicular to the longest particle axis. (The comparison of such points with the observed curve is rigorously valid only for a single size of particles, not for a distribution of sizes.) A factor f is chosen so that the maximum of $f(Q_1-Q_2)$ matches the maximum of the observed polarization. The circles in Figs. 2–6 give $f(Q_1-Q_2)$ plotted against $1/\lambda = x/2\pi a$, where $x = 2\pi a/\lambda$

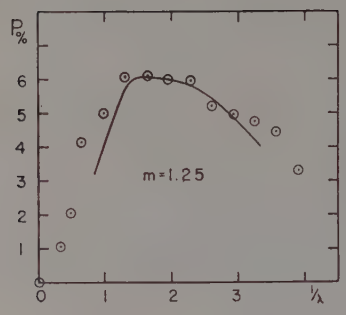

FIG. 2. The drawn line is copied from Fig. 1. The points with open circles are obtained from van de Hulst (1957), Fig. 71.

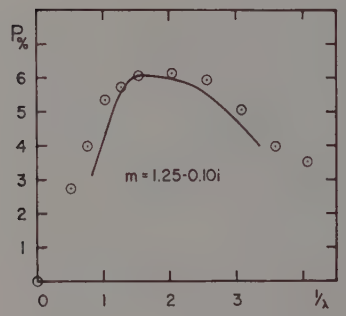

FIG. 3. Same caption as for Fig. 2.

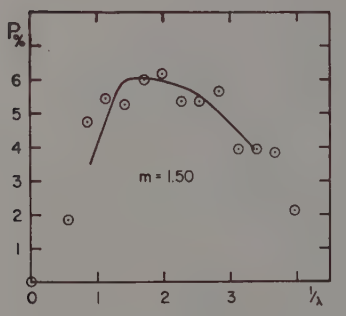

FIG. 4. Same caption as for Fig. 2.

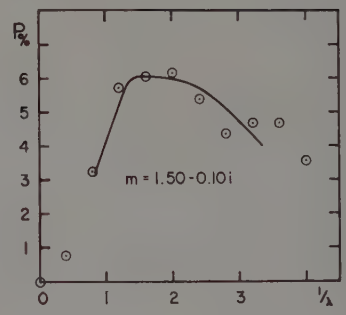

FIG. 5. Same caption for Fig. 2.

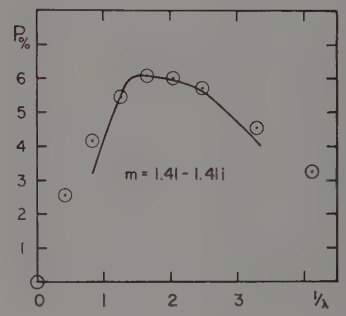

FIG. 6. Same capti as for Fig. 2, but fr van de Hulst (195 Fig. 69.

is the variable used by van de Hulst, and a is the radius of the cylinder. The value of a is chosen by trial and error to obtain the best fit.

The results of curve fitting and the resulting values of $2a$ are in Table III. Van de Hulst (1955) fitted these same extinction calculations to the observations interstellar reddening and he obtained the particle siz that are in the last column of Table III. The prese results appear consistent with those on interstel reddening. The cylinders are aligned, presumably the galactic magnetic field. Van de Hulst (1950) h indicated that the results of the calculations remain t same, but for the amount of polarization, when the lo cylinders are replaced by prolate spheroids. Mrs. van Smith kindly sent me a few calculations made refractive index $m=1.50-0.25\,i$, these also fit t observations and they give $2a=0.16$.

The fits appear equally close, within the uncertain of the method; for different values of the refracti index. It is therefore not possible from these data alo to decide between dielectric particles, metallic pa ticles, or a mixture with suitable size distribution. mixture of particles will be considered in a follow paper, using the observations on reflection nebulae

TABLE II. Normalized percentage polarization and galactic coordinates.

HD	Normalized polarization at 1/λ 1.01	1.46	1.79	2.38	2.79	3.08	l^{I}	b^{I}
161056	4.19	6.15	5.92	5.77	4.35	4.45	346°	+10°
154445	4.25	6.09	5.98	5.55	4.66	4.22	347	+21
183143	4.21	5.99	6.08	5.68	5.18:	4.28:	21	−1
198478	4.22	6.10	5.98	5.95	5.16	4.94	53	+1
21291	3.90	6.02	6.04	6.01	5.40	5.06:	109	+4
43384	4.62	...	6.03	...	5.36	...	156	+5
42379	4.24	...	6.03	...	6.65:	...	157	+3
41117	4.26	...	6.03	...	4.75	...	157	+1
Average	4.24	6.07	6.01	5.79	5.09	4.57	...	...

TABLE III. Comparison of the observations with calculati (van de Hulst 1957) for cylinders.

Substance	Refractive index	Figure in this paper	$2a$, from interstellar polarization	$2a$, fro interstel reddeni
Ices	1.25	2	0.49	0.70
Impure ices	1.25–0.10 i	3	0.31	...
Glass	1.50	4	0.28	0.35
Impure glass	1.50–0.10 i	5	0.20	0.32
	1.50–0.25 i	...	0.16	...
Metallic	1.41–1.41 i	6	0.05	0.07

l as the present results. However, the numerical cision of fitting the calculations to the peculiar ve of Fig. 1 is of the order of ± 0.02 in $2a$. A choice particle sizes and refractive indices will be quite ited by the observed wavelength dependence of erstellar polarization.

n conclusion, I would like to thank Mr. R. L. nfery for his help with reductions and illustrations.

REFERENCES

Behr. A. 1959, *Z. Astrophys.* **47**, 54 .
Davis, L. 1959, *Z. Astrophys.* **47**, 59.
Gehrels, T. 1960, *Astron. J.* **64**, 466 (Paper I).
Hulst, H. C. van de. 1950, *Astrophys. J.* **112**, 1.
——. 1955, *Mém. Soc. Roy. Sci. Liège*, 4th Ser., **15**, 403.
——. 1957, *Light Scattering by Small Particles* (John Wiley & Sons, Inc., New York).
Serkowski, K. 1960, *Lowell Obs. Bull.* **4**, 318.
Strömgren, B. 1956, *Astron. J.* **61**, 45.

E ASTRONOMICAL JOURNAL VOLUME 65, NUMBER 8 OCTOBER, 1960

Six-Color Photometry of Ten Classical Cepheids*

Sotirios N. Svolopoulos
Lick Observatory, University of California, Mt. Hamilton, California

(Received July 13, 1960)

Six-color observations of the cepheids U Aql, FF Aql, SU Cas, X Cyg, SU Cyg, DT Cyg, Y Oph, S Sge, Y Sgr, and T Vul, made with the 22-inch Tauchmann reflector, are presented. Light and color variations were determined in each of the six colors. Values of the phase retardation of the various light curves are given. The relation between the light range and the inverse wavelength was found to be linear in all cases, but with deviating points in the colors U, V, and I; the deviations are attributed to absorption in the outer layers of the stars. Eggen's type C cepheids are distinguished from those of types A and B of the same period in having a less steep slope in the relation between light range and inverse wavelength. Temperatures at maximum and minimum light have been derived from the six-color data: the average temperature range was found to be 1550° for type A and B cepheids and 750° for type C cepheids. Mean radii are given for four cepheids having accurate radial-velocity curves.

URING 1957 and 1958 a program of six-color observations of ten bright classical cepheids was ried out with the Tauchmann 22-inch reflector of Lick Observatory. An infrared-sensitive Lallemand otomultiplier, designated L II by Kron (1958a) was d with a combination of filters that will be described a future paper by Stebbins and Kron. Table I lists cepheids observed, in order of increasing period. e elements were taken chiefly from the *General alogue of Variable Stars* (Kukarkin *et al.* 1958). The heid types given in the last column have been taken n Eggen, Gascoigne, and Burr (1957).

The observations were made on dry, clear nights and standard extinction factors for each of the six colors were used in the reductions. The observed colors of the cepheids were reduced to the standard six-color system by comparison with the six-color data for nonvariable stars given by Stebbins and Kron (1956). The comparison stars used are listed in Table II. Two of these stars have been observed by Eggen (1955) in two colors, and their visual magnitudes in this system (V_E) were used in deriving visual magnitudes for the cepheids, by interpolation between green and violet. The observed visual magnitudes of the cepheids at maximum and minimum light are given in Table I. From 35 to 40 observations in each of the six colors for each cepheid, a mean light curve was drawn for each color. From the differences between each individual observation and the mean of the nearly simultaneous B, G, and R observations, a color curve was derived for each color. Figure 1 shows these curves for SU Cygni; they may be taken as typical examples of the data derived in this investigation. The mean deviations (in mag.) of the obser-

Table I. Cepheids observed in six colors.

tar	Epoch JD	Period (days)	V_E (max.)	V_E (min.)	ΔV_E	Cepheid type
Cas	2430404.134	1.949319	5.70	6.08	0.38	?
Cyg	24305.124	2.49934	5.60	5.90	0.30	C
Cyg	33095.944	3.845664	6.39	7.10	0.71	A
Vul	19372.151	4.435578	5.35	6.04	0.69	A
Aql	24703.115	4.470959	5.13	5.48	0.35	C
Sgr	25503.22	5.77335	5.28	6.08	0.80	A
Aql	10170.173	7.023836	5.98	6.78	0.80	B
Sge	29091.48	8.3821723	5.24	5.99	0.75	B
Cyg	21511.892	16.385680	5.82	6.89	1.07	B
Oph	08694.86	17.11884	5.77	6.29	0.52	C

Table II. Comparison stars.

Star	HD	Spectral type	V_E
15 Sagittae	190406	dGl	5.76
35 Cygni	193370	F5 Ib	
HR 7807	194335	B2 Vp	
44 Cygni	195593	F5 Iab	
ϵ Cygni	197989	K0 III	2.48

Lick Observatory Bulletin, No. 568.

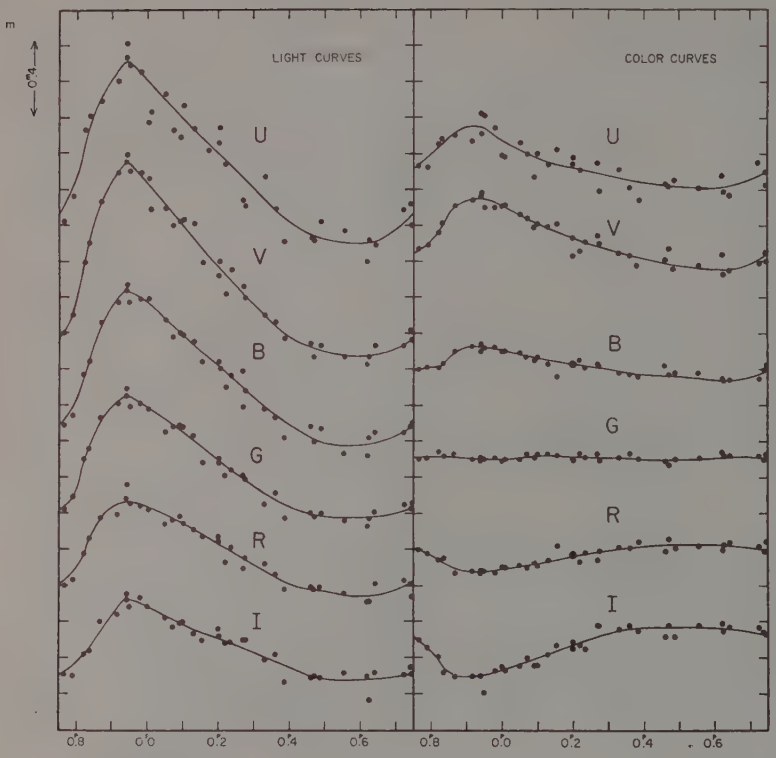

FIG. 1. Light and color curves for SU Cygni.

vations of SU Cygni from the mean curves are listed in Table III.

Table IV gives the brightness expressed in magnitudes in each of the observed six colors, taken from the mean light curves, at decimal phases. The median magnitude between maximum and minimum was used as the zero point. Also given in the table are the maximum and minimum magnitude and their differences. Table V gives the colors in the six-color system, as read from the smoothed color curves. The usual zero point, B+G+R=0, as previously stated, has been adopted. The slopes of the transformation lines for converting the observed colors to the standard system did not differ appreciably from unity. The extreme values were 1.07 for U and 0.91 for V.

Inspection of the light curves reveals, usually, a phase difference (infrared being later) between U and I. In Table VI an estimate of this phase retardation is given for each of the ten cepheids. It is difficult to judge the accuracy of this quantity, since it is determined from light curves in which the time of maximum light is often uncertain owing to observational errors. From the table, however, where the stars are listed in ord of increasing period, we see that there is no correlati between the phase difference and the period; also the is no correlation between the phase difference and t range of the mean light curve.

Miss Hack (1956) has shown that from 4000 to 6000 the light range of a cepheid is a linear function of t inverse wavelength in which it is measured. Plotti the ranges given in Table IV as a function of t reciprocal of the effective wavelength, we find that t points for the three colors B, G, and R lie on a straig line for all the cepheids, while the U point deviat from this straight line for some of them, and the V a I points for all. Figure 2 shows a plot of this type f SU Cygni.

The deviation of U is negative, i.e., the range magnitude is too small, presumably because of increas

TABLE III. Mean deviations of SU Cygni observations (in mag.).

	U	V	B	G	R	I
Light curves:	±0.06	±0.03	+0.03	±0.02	±0.03	+0.03
Color curves:	±0.05	±0.02	+0.01	±0.01	±0.01	±0.02

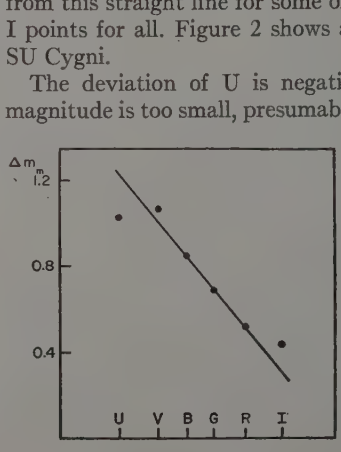

FIG. 2. Light range a function of μ^{-1} for Cygni.

TABLE IV. Six-color light curves of ten cepheids.

Phase	U	V	B	G	R	I
			SU Cassiopeiae			
0P0	−0.28	−0.29	−0.21	−0.18	−0.16	−0.17
0.1	−0.10	−0.18	−0.19	−0.14	−0.13	−0.17
0.2	+0.07	−0.05	−0.07	−0.05	−0.07	−0.13
0.3	+0.17	+0.08	+0.03	+0.03	+0.01	−0.08
0.4	+0.23	+0.19	+0.12	+0.10	+0.07	−0.02
0.5	+0.28	+0.28	+0.20	+0.16	+0.13	+0.04
0.6	+0.28	+0.29	+0.22	+0.18	+0.14	+0.14
0.7	+0.24	+0.20	+0.15	+0.14	+0.09	+0.12
0.8	+0.24	+0.06	+0.03	+0.06	+0.02	−0.02
0.9	+0.01	−0.10	−0.11	−0.08	−0.09	−0.11
Max	−0.30	−0.30	−0.22	−0.18	−0.16	−0.18
Min	+0.29	+0.30	+0.22	+0.18	+0.14	+0.18
n.-Max	0.59	0.60	0.44	0.36	0.31	0.36
			DT Cygni			
0P0	−0.23	−0.25	−0.18	−0.15	−0.12	−0.08
0.1	−0.22	−0.22	−0.16	−0.13	−0.11	−0.09
0.2	−0.09	−0.12	−0.10	−0.08	−0.09	−0.06
0.3	+0.06	0.00	−0.02	−0.01	−0.04	−0.02
0.4	+0.19	+0.13	+0.08	+0.06	+0.02	+0.03
0.5	+0.26	+0.24	+0.16	+0.12	+0.09	+0.07
0.6	+0.25	+0.23	+0.18	+0.15	+0.10	+0.09
0.7	+0.15	+0.10	+0.10	+0.10	+0.05	+0.06
0.8	+0.02	−0.03	−0.03	0.00	−0.01	+0.02
0.9	−0.10	−0.17	−0.13	−0.09	−0.07	−0.03
Max	−0.26	−0.26	−0.18	−0.15	−0.12	−0.10
Min.	+0.26	+0.26	+0.18	+0.15	+0.11	+0.09
n-Max	0.52	0.52	0.36	0.30	0.23	0.19
			SU Cygni			
0P0	−0.40	−0.43	−0.37	−0.28	−0.23	−0.18
0.1	−0.19	−0.19	−0.18	−0.15	−0.14	−0.08
0.2	0.00	+0.04	−0.02	+0.01	−0.02	0.00
0.3	+0.20	+0.25	+0.16	+0.16	+0.09	+0.07
0.4	+0.38	+0.43	+0.31	+0.27	+0.20	+0.15
0.5	+0.47	+0.50	+0.41	+0.32	+0.23	+0.21
0.6	+0.50	+0.53	+0.42	+0.32	+0.26	+0.22
0.7	+0.42	+0.49	+0.37	+0.30	+0.22	+0.20
0.8	+0.12	+0.19	+0.16	+0.16	+0.10	+0.12
0.9	−0.42	−0.46	−0.36	−0.30	−0.23	−0.14
Max	−0.53	−0.52	−0.43	−0.35	−0.26	−0.22
Min	+0.50	+0.51	+0.42	+0.34	+0.26	+0.22
n-Max	1.03	1.07	0.85	0.69	0.52	0.44
			T Vulpeculae			
0P0	−0.60	−0.57	−0.42	−0.32	−0.23	−0.17
0.1	−0.40	−0.39	−0.30	−0.23	−0.21	−0.17
0.2	−0.17	−0.17	−0.13	−0.11	−0.11	−0.14
0.3	+0.05	+0.06	+0.04	+0.01	−0.03	−0.05
0.4	+0.26	+0.25	+0.18	+0.12	+0.05	+0.05
0.5	+0.44	+0.40	+0.28	+0.22	+0.37	+0.12
0.6	+0.54	+0.52	+0.37	+0.30	+0.21	+0.17
0.7	+0.58	+0.56	+0.41	+0.32	+0.24	+0.17
0.8	+0.26	+0.37	+0.27	+0.23	+0.17	+0.13
0.9	−0.22	−0.20	−0.11	−0.02	−0.07	−0.01
Max	−0.60	−0.57	−0.42	−0.33	−0.25	−0.18
Min	+0.59	+0.56	+0.41	+0.32	+0.24	+0.17
n-Max	1.19	1.13	0.83	0.65	0.49	0.35
			FF Aquilae			
0P0	−0.30	−0.30	−0.20	−0.16	−0.12	−0.10
0.1	−0.15	−0.18	−0.14	−0.10	−0.08	−0.03
0.2	+0.01	0.00	+0.01	−0.01	0.00	+0.05
0.3	+0.21	+0.13	+0.09	+0.06	+0.05	+0.07
0.4	+0.25	+0.21	+0.14	+0.10	+0.05	+0.08
0.5	+0.30	+0.29	+0.18	+0.14	+0.07	+0.08
0.6	+0.25	+0.28	+0.18	+0.16	+0.10	+0.09
0.7	+0.17	+0.15	+0.12	+0.13	+0.10	+0.10
0.8	+0.01	−0.01	+0.01	0.00	+0.02	+0.08
0.9	−0.17	−0.17	−0.13	−0.10	−0.08	−0.03
Max	−0.31	−0.30	−0.20	−0.16	−0.12	−0.10
Min	+0.30	+0.29	+0.20	+0.16	+0.11	+0.10
n-Max	0.61	0.59	0.40	0.32	0.23	0.20
			Y Sagittarii			
0P0	−0.68	−0.62	−0.44	−0.34	−0.26	−0.24
0.1	−0.62	−0.51	−0.38	−0.33	−0.23	−0.18
0.2	−0.37	−0.19	−0.18	−0.17	−0.14	−0.07
0.3	−0.19	+0.03	0.00	−0.06	−0.07	−0.02
0.4	+0.05	+0.17	+0.12	+0.04	0.00	+0.04
0.5	+0.27	+0.33	+0.23	+0.14	+0.09	+0.11
0.6	+0.48	+0.53	+0.37	+0.24	+0.19	+0.18
0.7	+0.73	+0.64	+0.46	+0.34	+0.27	+0.25
0.8	+0.32	+0.43	+0.34	+0.27	+0.21	+0.19
0.9	−0.07	+0.03	+0.00	+0.01	+0.02	+0.06
Max	−0.74	−0.64	−0.47	−0.36	−0.27	−0.25
Min.	+0.73	+0.64	+0.46	+0.35	+0.27	+0.25
Min-ax	1.47	1.28	0.93	0.71	0.54	0.50
			U Aquilae			
0P0	−0.63	−0.63	−0.47	−0.39	−0.28	−0.18
0.1	−0.48	−0.45	−0.32	−0.22	−0.23	−0.19
0.2	−0.30	−0.25	−0.17	−0.10	−0.13	−0.12
0.3	−0.12	−0.11	−0.07	−0.02	−0.08	−0.09
0.4	+0.03	+0.04	+0.03	0.00	−0.08	−0.08
0.5	+0.20	+0.27	+0.20	+0.18	+0.06	−0.01
0.6	+0.44	+0.52	+0.33	+0.27	+0.16	+0.09
0.7	+0.63	+0.63	+0.45	+0.36	+0.24	+0.17
0.8	+0.52	+0.49	+0.41	+0.35	+0.27	+0.22
0.9	+0.08	−0.05	+0.01	+0.05	+0.07	+0.06
Max	−0.63	−0.63	−0.47	−0.39	−0.28	−0.23
Min	+0.63	+0.63	+0.47	+0.39	+0.28	+0.22
Min-Max	1.26	1.26	0.94	0.78	0.56	0.45
			S Sagittae			
0P0	−0.72	−0.63	−0.45	−0.34	−0.25	−0.20
0.1	−0.53	−0.39	−0.27	−0.21	−0.16	−0.11
0.2	−0.51	−0.36	−0.28	−0.29	−0.24	−0.19
0.3	−0.21	−0.15	−0.14	−0.15	−0.16	−0.17
0.4	+0.15	+0.17	+0.09	+0.02	−0.02	−0.06
0.5	+0.42	+0.39	+0.25	+0.16	+0.09	+0.04
0.6	+0.67	+0.58	+0.41	+0.33	+0.23	+0.15
0.7	+0.63	+0.60	+0.44	+0.33	+0.25	+0.19
0.8	+0.25	+0.30	+0.22	+0.19	+0.14	+0.15
0.9	−0.42	−0.30	−0.17	−0.11	−0.08	−0.01
Max	−0.74	−0.64	−0.46	−0.35	−0.26	−0.21
Min	+0.73	+0.64	+0.46	+0.35	+0.25	+0.20
Min-Max	1.47	1.28	0.92	0.70	0.51	0.41
			X Cygni			
0P0	−0.52	−0.41	−0.33	−0.19	−0.13	−0.05
0.1	−0.97	−0.90	−0.63	−0.48	−0.37	−0.32
0.2	−0.53	−0.46	−0.37	−0.33	−0.27	−0.20
0.3	0.00	−0.09	−0.12	−0.16	−0.15	−0.19
0.4	+0.46	+0.25	+0.10	0.00	−0.05	−0.13
0.5	+0.85	+0.57	+0.34	+0.19	+0.10	+0.02
0.6	+0.97	+0.80	+0.52	+0.36	+0.24	+0.13
0.7	+1.03	+0.94	+0.65	+0.49	+0.37	+0.24
0.8	+0.93	+0.87	+0.53	+0.38	+0.27	+0.19
0.85	+0.27	+0.42	+0.31	+0.27	+0.19	+0.12
0.9	+0.24	+0.18	+0.24	+0.21	+0.19	+0.11
0.94	+0.31	+0.53	+0.35	+0.35	+0.22	+0.20
Max	−1.09	−0.96	−0.65	−0.50	−0.39	−0.33
Min	+1.08	+0.95	+0.65	+0.49	+0.39:	+0.32
Min-Max	2.17	1.91	1.30	0.99	0.78:	0.65
			Y Ophiuchi			
0P0	−0.46	−0.42	−0.17	−0.13	−0.08	−0.06
0.1	−0.42	−0.36	−0.31	−0.22	−0.19	−0.14
0.2	−0.24	−0.19	−0.18	−0.12	−0.11	−0.08
0.3	0.00	−0.02	−0.03	−0.01	−0.02	−0.01
0.4	+0.19	+0.15	+0.12	+0.09	+0.05	+0.05
0.5	+0.37	+0.33	+0.25	+0.18	+0.13	+0.11
0.6	+0.48	+0.46	+0.32	+0.23	+0.18	+0.14
0.7	+0.46	+0.43	+0.31	+0.23	+0.19	+0.14
0.8	+0.25	+0.26	+0.23	+0.21	+0.16	+0.14
0.9	−0.08	−0.01	+0.04	+0.07	+0.06	+0.08
Max	−0.50	−0.48	−0.33	−0.24	−0.19	−0.14
Min	+0.49	+0.47	+0.32	+0.23	+0.19	+0.14
Min-Max	0.99	0.95	0.65	0.47	0.38	0.28

TABLE V. Color variations of ten cepheids.

Phase	U	V	B	G	R	I
			SU Cassiopeiae			
0P0	+0.36	−0.09	+0.03	0.00	−0.04	−0.09
0.1	+0.37	−0.02	+0.04	0.00	−0.04	−0.13
0.2	+0.41	+0.03	+0.05	0.00	−0.06	−0.17
0.3	+0.54	+0.07	+0.07	+0.01	−0.09	−0.20
0.4	+0.55	+0.11	+0.09	0.00	−0.10	−0.21
0.5	+0.55	+0.13	+0.11	−0.01	−0.11	−0.22
0.6	+0.54	+0.15	+0.14	−0.01	−0.12	−0.22
0.7	+0.49	+0.13	+0.12	−0.01	−0.11	−0.20
0.8	+0.39	+0.07	+0.07	0.00	−0.07	−0.16
0.9	+0.36	−0.02	+0.04	0.00	−0.05	−0.13
			DT Cygni			
0P0	−0.04	−0.28	−0.10	−0.01	+0.12	+0.20
0.1	−0.01	−0.25	−0.10	−0.01	+0.11	+0.17
0.2	+0.03	−0.22	−0.08	0.00	+0.08	+0.14
0.3	+0.09	−0.19	−0.07	0.00	+0.06	+0.11
0.4	+0.14	−0.11	−0.04	0.00	+0.04	+0.09
0.5	+0.15	−0.08	−0.04	0.00	+0.03	+0.07
0.6	+0.12	−0.10	−0.03	−0.01	+0.04	+0.06
0.7	+0.08	−0.14	−0.05	−0.02	+0.06	+0.12
0.8	+0.04	−0.21	−0.08	−0.01	+0.10	+0.17
0.9	0.00	−0.26	−0.10	−0.01	+0.11	+0.20
			SU Cygni			
0P0	−0.07	−0.31	−0.10	0.00	+0.11	+0.17
0.1	+0.03	−0.21	−0.06	−0.02	+0.08	+0.10
0.2	+0.08	−0.13	−0.03	−0.01	+0.04	+0.03
0.3	+0.12	−0.07	0.00	−0.01	+0.01	−0.04
0.4	+0.16	−0.02	+0.03	0.00	−0.02	−0.07
0.5	+0.18	+0.02	+0.04	0.00	−0.03	−0.07
0.6	+0.18	+0.04	+0.05	−0.01	−0.03	−0.07
0.7	+0.14	+0.01	+0.04	−0.02	−0.01	−0.05
0.8	0.00	−0.12	−0.01	−0.02	+0.04	+0.07
0.9	−0.15	−0.34	−0.12	−0.01	+0.12	+0.20
			T Vulpeculae			
0P0	−0.01	−0.27	−0.11	−0.01	+0.13	+0.19
0.1	+0.08	−0.19	−0.08	0.00	+0.08	+0.14
0.2	+0.19	−0.10	−0.03	−0.01	+0.04	+0.07
0.3	+0.29	−0.01	+0.01	−0.02	0.00	0.00
0.4	+0.38	+0.07	+0.04	−0.01	−0.03	−0.06
0.5	+0.44	+0.13	+0.06	−0.01	−0.04	−0.10
0.6	+0.48	+0.16	+0.06	−0.01	−0.04	−0.09
0.7	+0.46	+0.16	+0.06	−0.01	−0.05	−0.06
0.8	+0.35	+0.06	+0.02	−0.01	−0.01	−0.01
0.9	+0.09	−0.17	−0.05	−0.01	+0.07	+0.13
			FF Aquilae			
0P0	+0.39	0.00	+0.02	−0.01	−0.01	−0.12
0.1	+0.47	+0.04	+0.05	0.00	−0.05	−0.17
0.2	+0.54	+0.11	+0.08	0.00	−0.07	−0.20
0.3	+0.59	+0.14	+0.09	0.00	−0.08	−0.23
0.4	+0.62	+0.16	+0.11	0.00	−0.12	−0.25
0.5	+0.63	+0.19	+0.12	0.00	−0.13	−0.26
0.6	+0.61	+0.19	+0.13	0.00	−0.13	−0.27
0.7	+0.58	+0.17	+0.10	0.00	−0.10	−0.24
0.8	+0.51	+0.11	+0.07	0.00	−0.08	−0.19
0.9	+0.45	+0.05	+0.05	−0.01	−0.05	−0.14

Phase	U	V	B	G	R	I
			Y Sagittarii			
0P0	+0.52	+0.02	+0.02	0.00	−0.02	−0.
0.1	+0.50	+0.08	+0.04	0.00	−0.05	−0.
0.2	+0.52	+0.19	+0.09	0.00	−0.10	−0.
0.3	+0.60	+0.28	+0.15	−0.01	−0.15	−0.
0.4	+0.73	+0.38	+0.19	−0.01	−0.19	−0.
0.5	+0.85	+0.43	+0.21	0.00	−0.21	−0.
0.6	+0.98	+0.48	+0.22	0.00	−0.22	−0.
0.7	+1.05	+0.52	+0.23	0.00	−0.23	−0.
0.8	+0.81	+0.40	+0.18	+0.01	−0.19	−0.
0.9	+0.61	+0.22	+0.11	+0.01	−0.13	−0.
			U Aquilae			
0P0	+0.88	+0.27	+0.18	0.00	−0.17	−0.
0.1	+0.89	+0.32	+0.19	0.00	−0.20	−0.
0.2	+0.95	+0.40	+0.22	0.00	−0.23	−0.
0.3	+1.03	+0.47	+0.28	0.00	−0.28	−0.
0.4	+1.12	+0.53	+0.31	0.00	−0.32	−0.
0.5	+1.21	+0.62	+0.32	0.00	−0.33	−0.
0.6	+1.28	+0.71	+0.34	0.00	−0.34	−0.
0.7	+1.30	+0.72	+0.34	0.00	−0.34	−0.
0.8	+1.23	+0.61	+0.31	0.00	−0.32	−0.
0.9	+1.01	+0.41	+0.25	0.00	−0.25	−0.
			S Sagittae			
0P0	+0.25	−0.08	−0.04	0.00	+0.04	0.
0.1	+0.43	+0.05	+0.02	0.00	−0.01	−0.
0.2	+0.43	+0.08	+0.04	0.00	−0.04	−0.
0.3	+0.60	+0.19	+0.07	0.00	−0.08	−0.
0.4	+0.77	+0.31	+0.12	−0.01	−0.12	−0.
0.5	+0.95	+0.39	+0.15	−0.01	−0.14	−0.
0.6	+1.09	+0.45	+0.18	−0.01	−0.16	−0.
0.7	+1.05	+0.41	+0.17	−0.01	−0.15	−0.
0.8	+0.68	+0.27	+0.10	0.00	−0.10	−0.
0.9	+0.34	+0.04	+0.02	0.00	−0.02	−0.
			X Cygni			
0P0	+0.91	+0.30	+0.18	−0.01	−0.16	−0.
0.1	+0.72	+0.24	+0.13	−0.01	−0.12	−0.
0.2	+0.97	+0.44	+0.21	−0.01	−0.20	−0.
0.3	+1.27	+0.64	+0.29	−0.02	−0.28	−0.
0.4	+1.66	+0.78	+0.34	−0.02	−0.31	−0.
0.5	+1.82	+0.88	+0.38	−0.02	−0.35	−0.
0.6	+1.81	+0.93	+0.41	−0.02	−0.40	−0.
0.7	+1.81	+0.97	+0.40	−0.01	−.040	−0.
0.8	+1.75	+0.97	+0.36	+0.01	−0.37	−0.
0.85	+1.15	+0.70	+0.31	+0.02	−0.33	−0.
0.9	+1.20	+0.54	+0.30	+0.01	−0.30	−0.
0.94	+1.23	+0.75	+0.29	+0.03	−0.32	−0.
			Y Ophiuchi			
0P0	+1.36	+0.76	+0.45	+0.03	−0.49	−1.
0.1	+1.54	+0.84	+0.43	+0.02	−0.44	−1.
0.2	+1.70	+0.90	+0.47	+0.02	−0.50	−1.
0.3	+1.84	+0.95	+0.51	+0.02	−0.54	−1.
0.4	+1.95	+1.02	+0.55	+0.02	−0.58	−1.
0.5	+2.00	+1.11	+0.56	+0.02	−0.59	−1.
0.6	+2.00	+1.15	+0.57	+0.01	−0.59	−1.
0.7	+1.95	+1.08	+0.56	+0.01	−0.58	−1.
0.8	+1.83	+0.99	+0.54	+0.02	−0.57	−1.
0.9	+1.63	+0.89	+0.50	+0.03	−0.54	−1.

hydrogen absorption during the maximum phase. The deviation of V is positive and is a function of the spectral type at minimum light as given by Code (1947), as well as of the range of the spectral type from maximum to minimum. It is probably due to the presence of numerous metallic absorption lines in this spectral region, which increase in strength at minimum light. The regio of the I color is near the maximum of the negativ hydrogen-ion absorption, and the positive deviation o the I point may be due chiefly to changes in that ab sorption.

If we derive from the above-mentioned plots th

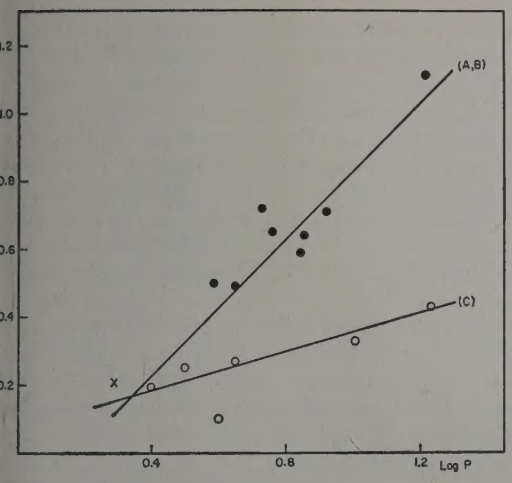

FIG. 3. Slope of the range-reciprocal wavelength relation as a ction of the logarithm of the period. Spots: type A and B heids; circles: type C cepheids; cross: SU Cassiopeiae.

pes of the straight lines, using only the three colors B, and R, and plot these values, which we shall call s and which are given in Table VII, as a function of e logarithm of the period, we find that the various ints define two straight lines, well separated from ch other, as can be seen in Fig. 3. This diagram also ludes points for δ Cep (type A), η Aql (type B), UMi (type C) observed by Stebbins (1953 and 1946), d for SZ Tau and ζ Gem (both type C), taken from ent work by the writer (Svolopoulos 1959), The per line has the equation $k=1.00\cdot\log P-0.175$, and ates to A and B-type cepheids, while the lower has e equation $k=0.275\cdot\log P+0.075$, and relates to type cepheids. The 15 stars plotted in Fig. 3 are scarcely equate to establish such a separation for all cepheids; vertheless, the scatter in such a plot should be less an that in the plots attempting to separate the various

TABLE VI. Phase retardation of light maximum between U and I.

SU Cas	0^{p}03	Y Sgr	0.00
DT Cyg	0.05	U Aql	0.06
SU Cyg	0.01	S Sge	0.03
T Vul	0.04	X Cyg	0.02
FF Aql	0.02	Y Oph	0.06

types of cepheids by use of spectral regions that are more affected by hydrogen or metallic-line absorption. For example, the plot given by Eggen (1951) relating photographic range to period will be more affected by such absorption; this effect is shown by the deviations of our V points from a linear plot. The physical interpretation of the result shown in Fig. 3 is not clear to the writer.

We have attempted to compute the values of k directly from our color data in a different manner. For a blackbody, the Wien approximation gives for the light range, A_λ, of a variable star (Hack 1956):

$$A_\lambda=5\log\frac{r_{\max}}{r_{\min}}-\frac{c}{\lambda}\left(\frac{1}{T_{\max}}-\frac{1}{T_{\min}}\right),$$

where $r_{\max}$ and $r_{\min}$ are the maximum and minimum radii and $T_{\max}$ and $T_{\min}$ are the corresponding surface temperatures. We then have

$$k_{\text{comp}}=-c\left(\frac{1}{T_{\max}}-\frac{1}{T_{\min}}\right).$$

The color temperatures of the various cepheids at both maximum and minimum light were computed directly from the observed six-color data in the following manner. The B-R color differences, which refer to a range of spectrum not much affected by absorption lines and bands, were first corrected for color excess, and then the corresponding blackbody temperatures were derived from the table given by Stebbins and Whitford (1945).

TABLE VII. Temperature data for fifteen cepheids.

Star	Cepheid type	$CE_{(B-R)}$	$(B-R)_{\max}$	$(B-R)_{\min}$	$T_{\max}$	$T_{\min}$	k_{obs}	k_{comp}
SU Cas	?	+0^{m}37	−0.30	−0.12	6650	5900	0.21	0.30
DT Cyg	C	+0.13	−0.35	−0.20	6900	6200	0.20	0.26
SZ Tau	C	+0.48	−0.28	−0.07:	6550	5900:	0.25	0.26
SU Cyg	A	+0.30	−0.49	−0.20	7650	6200	0.50	0.48
α UMi	C	+0.10	−0.26	−0.20	6750	6200	0.10	0.21
T Vul	A	+0.23	−0.46	−0.11	7500	5850	0.49	0.59
FF Aql	C	+0.40	−0.36	−0.16	6950	6050	0.27	0.33
δ Cep	A	+0.22	−0.51	−0.02	7800	5600	0.72	0.79
Y Sgr	A	+0.34	−0.30	+0.12	6650	5150	0.65	0.69
U Aql	B	+0.51	−0.17	+0.16	6100	5000	0.59	0.56
η Aql	B	+0.30	−0.37	+0.06	7000	5300	0.64	0.72
S Sge	B	+0.20	−0.23	+0.15	6300	5050	0.71	0.61
ζ Gem	C	+0.17	−0.16	+0.09	6000	5200	0.33	0.49
X Cyg	B	+0.41	−0.17	+0.39	6100	4550	1.11	0.87
Y Oph	C	+0.85	+0.03	+0.29	5600	4750	0.43	0.49

TABLE VIII. Radius variations for four cepheids.

Phase	dr/dt (km/sec)	$r-R$ (10^5 km)	Phase	dr/dt (km/sec)	$r-R$ (10^5 km)
DT Cygni			T Vulpeculae		
0P0	+9.6	−1.7	0P0	+25.3	−8.9
0.1	+11.2	+0.6	0.1	+20.2	+0.0
0.2	+5.4	+2.3	0.2	+12.7	+6.3
0.3	+1.0	+3.0	0.3	+5.5	+9.9
0.4	−3.0	+2.8	0.4	−1.8	+10.6
0.5	−6.1	+1.8	0.5	−8.9	+8.5
0.6	−8.2	+0.2	0.6	−15.5	+3.8
0.7	−10.7	−1.7	0.7	−20.6	−3.3
0.8	−4.9	−3.5	0.8	−19.8	−11.2
0.9	+5.1	−3.5	0.9	+3.8	−15.6
SU Cygni			Y Ophiuchi		
0P0	+24.7	−4.5	0P0	+5.1	−23.0
0.1	+20.5	+3.2	0.1	+10.3	−10.0
0.2	+12.0	+8.6	0.2	+12.0	+6.0
0.3	+3.5	+11.2	0.3	+7.5	+21.0
0.4	−4.9	+11.0	0.4	+0.3	+27.0
0.5	−16.2	+7.5	0.5	−5.8	+23.0
0.6	−27.5	+0.2	0.6	−10.7	+10.0
0.7	−27.5	−9.6	0.7	−11.1	−7.0
0.8	−4.9	−15.6	0.8	−6.9	−20.0
0.9	+23.3	−12.5	0.9	−1.3	−26.3

The color excesses in B-R were derived from the **P-V** color excesses given in a recent paper by Kron and Svolopoulos (1959), in the same way as those in **P-V** were derived from those in V-B by Kron (1958b). The color excesses, B-R values, derived temperatures, and computed values of k are given in Table VII. The computed values of k are, generally, somewhat larger than the observed values, especially for the type C cepheids, but in view of the uncertainties in the computation the agreement seems fairly satisfactory. The temperatures and computed k values are, of course, quite dependent on the interstellar absorption values adopted.

The temperatures of the type C cepheids appear to be somewhat lower at maximum light and somewhat higher at minimum light than those of the type A and B cepheids of similar period. The temperature ranges are much larger for the A- and B-type cepheids than for those of C-type, as anticipated: $\Delta T_{AB}=1550°$, $\Delta T_C=750°$; the mean temperatures of the three types of cepheids at the same period do not appear to differ appreciably, within the errors of the present determinations.

Combining the relations giving the light range as a function of inverse wavelength and the straight line of Fig. 3 for cepheids of types A and B ,we obtain

$$\Delta m=(\log P-0.175)\cdot\mu^{-1}-1.05\log P+0.42,$$

which gives the light range as a function of the period and the wavelength. A check of this formula with the observational data for the colors B, G, and R was quite satisfactory for all of the cepheids discussed here. Also for U—for those stars unaffected by absorption in that color—the formula was also satisfactory. Since no stars of period around 9 days were measured, it was not possible to test a possible discontinuity of the relation there, as others have suspected (Ledoux and Walra 1958). As only a few type C variables are include our list, such a relation was not derived for them.

For four of the cepheids that have reliable rad velocity curves, an attempt was made to determine mean radius by applying the Wesselink (1946) meth in the same way as Stebbins (1953) had applie previously. The rate of variation of the cepheid's was computed from the radial-velocity curve assum a reduction factor of 24/17, which is appropriate intermediate limb darkening. The radial-velocity cu used were corrected in phase, utilizing the element the present photometric observations. Numerical i gration then gave the radius displacements, wh when combined with the difference in magnit between two phases of equal color, gave the m radius. The variation of the radius, dr/dt, and radius displacements, $r-R$, are given in Table VIII the four cepheids. The displacement curves are plo

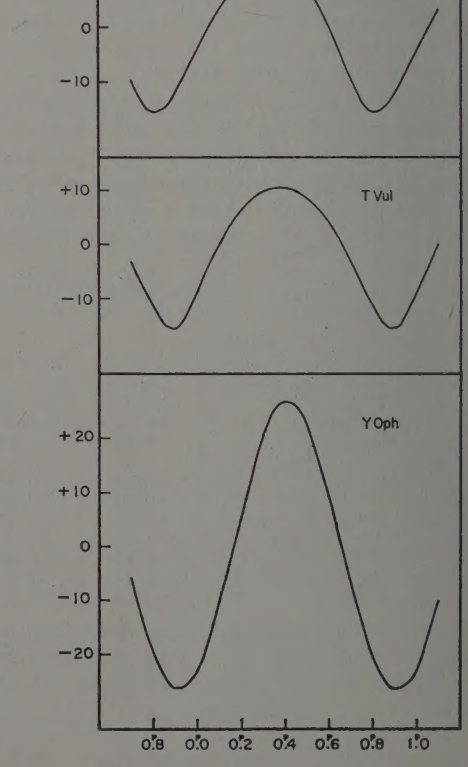

FIG. 4. Radius displacement curves for four cepheids.

TABLE IX. Computation of cepheid radii.

DT Cygni					
Phase 1	0^{p}05	0^{p}15	0^{p}40	0^{p}45	
Phase 2	0^{p}895	0^{p}85	0^{p}63	0^{p}60	
Δm	0^{m}060	0^{m}068	0^{m}072	0^{m}050	
n	1.0280	1.0318	1.0337	1.0239	
$\Delta r_1 \cdot 10^{-5}$ km	−0.5	+1.6	+2.7	+2.3	
$\Delta r_2 \cdot 10^{-5}$ km	−3.6	−3.8	−0.4	+0.2	
$R \cdot 10^{-7}$ km	1.1	1.7	2.1	0.9	
Weight	1	3	2	2	
SU Cygni					
Phase 1	0^{p}00	0^{p}20	0^{p}30		
Phase 2	0^{p}87	0^{p}805	0^{p}77		
Δm	0^{m}075	0.116	0.092		
n	1.035	1.055	1.0435		
$\Delta r_1 \cdot 10^{-5}$ km	−4.5	+8.5	+11.2		
$\Delta r_2 \cdot 10^{-5}$ km	−14.7	−15.6	−14.8		
$R \cdot 10^{-7}$ km	3.06	4.54	6.13		
Weight	1	4	2		
T Vulpeculae					
Phase 1	0^{p}15	0^{p}25	0^{p}35	0^{p}40	0^{p}45
Phase 2	0^{p}89	0^{p}85	0^{p}815	0^{p}795	0^{p}775
Δm	0^{m}176	0^{m}144	0^{m}122	0^{m}112	0^{m}094
n	1.0845	1.0686	1.058	1.053	1.044
$\Delta r_1 \cdot 10^{-5}$ km	+3.5	+8.4	+10.5	+10.6	+9.8
$\Delta r_2 \cdot 10^{-5}$ km	−15.6	−14.6	−12.3	−10.8	−9.2
$R \cdot 10^{-7}$ km	2.4	3.5	4.1	4.2	4.4
Weight	2	3	3	3	2
Y Ophiuchi					
Phase 1	0^{p}15	0^{p}20	0^{p}30	0^{p}40	
Phase 2	0^{p}91	0^{p}90	0^{p}85	0^{p}77	
Δm	0^{m}252	0^{m}186	0^{m}158	0^{m}130	
n	1.123	1^{m}090	1.075	1.062	
$\Delta r_1 \cdot 10^{-5}$ km	−1.0	+6.0	+21.0	+27.0	
$\Delta r_2 \cdot 10^{-5}$ km	−26.5	−26.4	−24.0	−16.3	
$R \cdot 10^{-7}$ km	2.34	3.81	6.40	7.10	
Weight	1	1	1	1	

ig. 4. Table IX gives the pairs of phases of equal
in the ascending and the descending branches
were matched, and also details of the computation
ie radius by the formula

$$R=\frac{\Delta r_1-n\Delta r_2}{n-1},$$

re Δr_1, and Δr_2 are the radius displacements at the
matched phases 1 and 2, and n is computed from
relation $\log n=0.2\,\Delta m$, where Δm is the mean dif-
ice in magnitude in the four colors V, B, G, and R.
the matched phases 1 and 2 are not at the extreme
ts of maximum and minimum light, but between
, the deviation in Δm of V, because of the metallic-
absorption, is smaller than the observational error,
ere is no reason not to use the V color in this radius
putation. For the same reason the colors U and I
occasionally used.) Table X gives the mean,
mum, and minimum radii of the stars, and the
ional variation in the radius. The probable errors
ie weighted means of the individual values of R
lso given in the table. For Y Ophiuchi the results
n in Table X agree very well with the computation
bt (1954), who used Eggen's two-color photometric
rvations.

For SU Cassiopeiae the application of the Wesselink method led to unsatisfactory results. SU Cassiopeiae is bluer in a part of the descending branch near minimum light than it is in the ascending branch at points where the brightness, as observed in the four colors used, is the same; the computation thus gives a negative radius near minimum light and the mean radius is indeterminate by this method. It would seem that this star must deviate considerably from a blackbody, as in cases previously discussed by Arp (1957).

From the radii and the radius-displacement curves, the light variation produced by the changing surface area of each of the four stars was computed. Subtracting the surface-area effect from the mean observed light

TABLE X. Summary of radius data.

Star	$(R/R_\odot)_{mean}$	R_{max} (10^7 km)	R_{min} (10^7 km)	dR/R	Reference for radial-velocity curve
DT Cyg	22±3	1.53	1.46	0.05	Grasberger and Herbig (1952)
SU Cyg	70±8	5.0	4.7	0.06	Becker and Strohmeier (1942)
T Vul	55±3	3.9	3.6	0.07	Lüst-Kulka (1954)
Y Oph	70±10	5.2	4.6	0.11	Abt (1954)

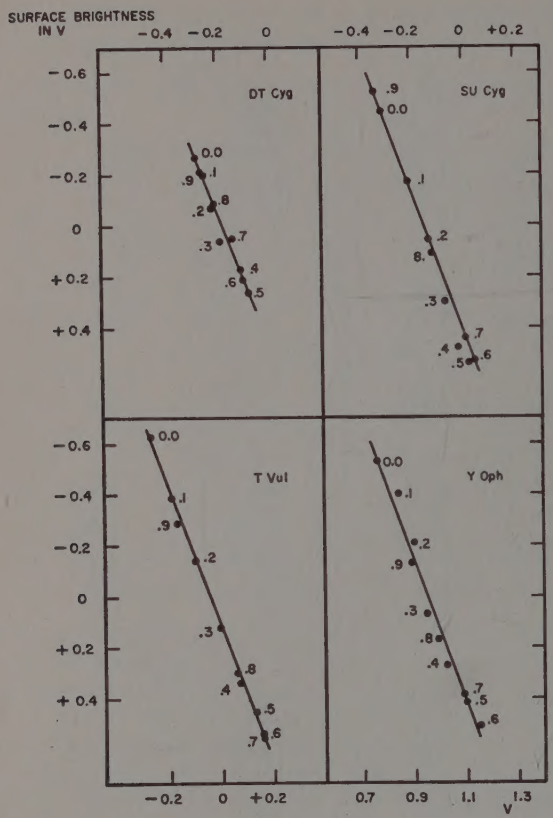

FIG. 5. Surface brightness in V as a function of the color V.

curves, we obtain the variation of the surface brightness with phase. A plot of the surface brightness in the color V against the V color for the various phases gave a straight line for each star included in Table X (Fig. 5). This result is consistent with the assumption of the Wesselink method that the surface brightness is a single-valued function of the color. The effect of th metallic-line absorption on the V magnitude is to small to appear in Fig. 5.

ACKNOWLEDGMENTS

I am indebted to Dr. G. E. Kron for his suggestio of this investigation, and acknowledge with pleasur his valuable assistance and encouragement. I am als indebted to Dr. C. D. Shane for extending to me th use of the observatory facilities, to Dr. A. E. Whitford Director of the Lick Observatory, for his interest an helpful suggestions in the presentation of this work, an to Dr. W. P. Bidelman for substantial editorial as sistance.

REFERENCES

Abt, H. A. 1954, *Publs. Astron. Soc. Pacific* **66**, 65.
Arp, H. C. 1957, *Astron. J.* **62**, 134.
Becker, W. and Strohmeier, W. 1942, *Z. Astrophys.* **21**, 295.
Code, A. D. 1947, *Astrophys. J.* **106**, 309.
Eggen, O. J. 1951, *Astrophys. J.* **113**, 367.
——. 1955, *Astron. J.* **60**, 65.
Eggen, O. J., Gascoigne, S.C.B., and Burr, E. J. 1957, *Monthl Notices Roy. Astron. Soc.* **117**, 406.
Grasberger, W. H. and Herbig, G. H. 1952, *Publs. Astron. So Pacific* **64**, 28.
Hack, M. 1956, in *Vistas in Astronomy* (Pergamon Press, Londo Vol. II, p. 1150.
Kron, G. E. 1958a, *Publs. Astron. Soc. Pacific* **70**, 285.
——. 1958b, *ibid.*, **70**, 561.
Kron, G. E., and Svolopoulos, S. N. 1959, *Publs. Astron. So Pacific* **71**, 126.
Kukarkin, B. V., Parenago, P. P., Efremov, Yu. I., and Kholopo P. N. 1958, *General Catalogue of Variable Stars* (Academy Science, Moscow).
Ledoux, P. and Walraven, Th. 1958, in *Handbuch der Physik* Vo 51, S. Flügge, ed. (Springer-Verlag, Berlin) p. 373.
Lüst-Kulka, R. 1954, *Z. Astrophys.* **33**, 211.
Stebbins, J. and Whitford, A. E. 1945, *Astrophys. J.* **102**, 318.
——. 1946, *ibid.* **103**, 108.
——. 1953, *Publs. Astron. Soc. Pacific* **65**, 118.
Stebbins, J., and Kron, G. E. 1956, *Astrophys. J.* **123**, 440.
——. 1957, *ibid.* **126**, 266.
Svolopoulos, S. N. 1959, thesis, Athens.
Wesselink, A. J. 1946, *Bull. Astron. Inst. Neth.* **10**, 91.